

A study of interjoint coordination
during locomotion after spinal cord injury

April 2022

Yuta Sato

A Thesis for the Degree of Ph.D. in Science

A study of interjoint coordination
during locomotion after spinal cord injury

April 2022

Graduate School of Science and Technology

Keio University

Yuta Sato

Contents

Chapter 1: General introduction	1
1.1. Modular structures controlling redundancy in the musculoskeletal system..	3
1.2. Altered locomotor patterns in central lesions	7
<i>1.2.1. Modular structure in supraspinal injury patients.....</i>	<i>8</i>
<i>1.2.2. Modular structure in spinal cord injury patients.....</i>	<i>9</i>
1.3. Limitation in human locomotor study	12
1.4. Difference in rodent, non-human primate, and human for locomotion after SCI	15
1.5. Purpose of the Dissertation	16
 Chapter 2: Functional reorganization of locomotor kinematic synergies reflects the neuropathology in a mouse model of spinal cord injury	 19
2.1. Introduction	19
2.2. Material and Methods	21
<i>2.2.1. Animals</i>	<i>21</i>
<i>2.2.2. Experimental procedure</i>	<i>21</i>
<i>2.2.3. Kinematics Recording.....</i>	<i>22</i>
<i>2.2.4. Kinematic synergy extraction</i>	<i>23</i>
<i>2.2.5. Hierarchical clustering.....</i>	<i>25</i>
<i>2.2.6. Similarity analysis</i>	<i>25</i>
<i>2.2.7. Tissue processing and analysis</i>	<i>26</i>
2.3. Results.....	26

2.3.1. Kinematic synergies in intact mice	26
2.3.2. Kinematic synergies in SCI mice	29
2.3.3. Morphometric analysis of SCI.....	34
2.4. Discussion	35
Chapter 3: Preserved Intersegmental Coordination of	
Locomotion in Spinal Cord Injury Common Marmosets	39
3.1. Introduction	39
3.2. Material and Methods	41
3.2.1. Animals	41
3.2.2. Experimental procedures	41
3.2.3. Open filed scoring	42
3.2.4. Kinematic recording	42
3.2.5. Endpoint trajectory.....	45
3.2.6. Joint angle	45
3.2.7. Planar covariation of elevation angle	46
3.2.8. Correlation between hip-ankle distance and place orientation	46
3.2.9. Histology.....	47
3.3. Results.....	47
3.3.1. Functional recovery after SCI	47
3.3.2. Endpoint trajectory.....	48
3.3.3. Joint angle	52
3.3.4. Planar covariation of the segment elevation angles	54
3.4. Discussion	60

Chapter 4: Conclusion 63

Acknowledgements

References 71

List of Figures

Figure 1-1. Musculoskeletal models of bipedal (left) and quadrupedal (right) locomotion	3
Figure 1-2. Pattern of intersegmental coordination in human (A) and monkey (B)	5
Figure 1-3. Schematic model of basic activation patterns.....	6
Figure 1-4. Number of modules to reconstruct muscle activity during locomotion.....	9
Figure 1-5. Patterns of intersegmental kinematic coordination.....	10
Figure 1-6. Kinematics and surface EMG during locomotion	11
Figure 1-7. Descending pathways in the spinal cord of a mouse	13
Figure 1-8. Plasticity phenomena induced by SCI	15
Figure 1-9. Deep learning based kinematics in intact and SCI mice.....	17
Figure 2-1. Kinematic synergies in intact mice	28
Figure 2-2. Kinematic synergies in SCI mice, grouped into three groups	30
Figure 2-3. The absolute values of coefficient calculated as a liner combination.....	32
Figure 2-4. The scores in intact mice and group 1	34
Figure 2-5. Spared tissue at the lesion epicenter	35
Figure 3-1. Schematic of runway for kinematic recording.....	43
Figure 3-2. Locations of the tracked joints.....	44
Figure 3-3. Lesion extent and open field scoring.	48
Figure 3-4. Changes in basic gait parameters and footfalls.....	50
Figure 3-5. Changes in endpoint trajectory during each session.....	51
Figure 3-6. Principal component analysis applied to 12 computed joint angle parameters	53
Figure 3-7. Planar covariation of the elevation angles	56

Figure 3-8. Orientation of the covariation plane for segment elevation angle.....	58
Figure 3-9. Positional relationship of hip and ankle joints.....	59
Figure 4-1. Schematic representation of new connection after SCI in rat.....	65

List of Tables

Table 1-1. Key muscle function corresponding to each segment of the spinal cord	2
Table 3-1. Lower Limb section of the open field rating scale	42
Table 3-2. Number of trials.....	43

Abbreviations

3-D	3-dimensional
CNS	Central nervous system
CST	Corticospinal tract
DTI	Diffusion tensor imaging
EMG	Electromyography
MRI	Magnetic resonance imaging
MTP	Metatarsophalangeal
NMF	Non-negative matrix factorization
PA	Parallel analysis
PC	Principal component
PCA	Principal component analysis
Pre	Pre-operation
PO2w	Post-operation at two weeks
PO6w	Post-operation at six weeks
PO12w	Post-operation at twelve weeks
PV	Percentage of variance
RST	Reticulospinal tract
SCI	Spinal cord injury
SD	Standard deviation

Chapter 1: General introduction

Understanding locomotor responses after neurological lesions is fundamental to explore the essence of flexible adaptation of the nervous system and to develop innovative neurological rehabilitation. In particular, spinal cord injury (SCI) is an important research target for this understanding in terms of the disruption of communication between supraspinal centers and spinal circuit. The central nervous system (CNS) controls numerous muscles and joints using common motor commands and produces coordinated joint movement. However, no evaluation measure that focuses on coordinated movement has been tested so far. In clinical environment, a clinician determines the affected segments of the spinal cord by an examination of myotomes (International Standards for Neurological Classification of Spinal Cord Injury; ISNCSCI) (Kirshblum et al., 2011), that is, key muscle function strength corresponding to each segment (but not coordination of movement) is just simply examined (Table 1-1).

Table 1-1. Key muscle function corresponding to each segment of the spinal cord

Level	Key muscle function
C5	Elbow flexors
C6	Wrist extensors
C7	Elbow extensors
C8	Finger flexors
T1	Small finger abductors
L2	Hip flexors
L3	Knee extensors
L4	Ankle dorsiflexors
L5	Long toe extensors
S1	Ankle plantar flexors

On the other hand, several kinematic studies have investigated the relationship between changes in superficial parameters such as stride length and joint angles during locomotion and neuropathology of the spinal cord in animal model; however, little is known about altered coordinated movement that underlies the generation of such gait parameters. Therefore, the author investigated the gait disturbance that occurs after SCI from the perspective of CNS as a gait controller. In this chapter, the author first summarizes how the CNS controls the redundant musculoskeletal systems during locomotion, then how locomotor output patterns are affected by CNS lesions. The purpose of the present dissertation was also described. In the following Chapter 2, the author investigated the differences in locomotor output patterns from CNS in mice with varying degrees of injury to obtain proof of the analysis. In order to verify whether the analysis method is adaptable to humans in the future, Chapter 3 describes the plastic change of locomotor output patterns after SCI in non-human primates, common marmosets. The overall conclusion

and future prospect of the present study are mentioned in Chapter 4.

1.1. Modular structures controlling redundancy in the musculoskeletal system

Terrestrial locomotion in animals has evolved in widely different designs adapted the habitat of each species (Grillner, 1981). The number of limbs (bipedal vs. quadrupedal), limb length, shape, and mass of limbs may differ, resulting in different locomotion styles. Nevertheless, it is believed that there is a common principle of organization that underlie the diversity of locomotor styles across species (Catavittello et al., 2018). With regard to neuromuscular control, musculoskeletal systems are composed of numerous muscles and joints, and it is necessary to provide control commands to all of them to walk according to the environment (Figure 1-1) (Aoi and Funato, 2016).

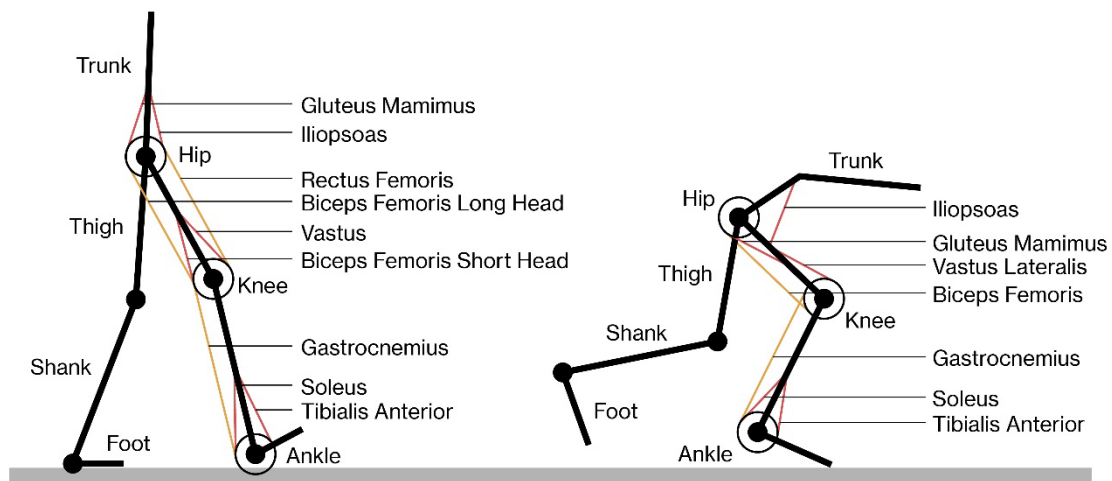


Figure 1-1. Musculoskeletal models of bipedal (left) and quadrupedal (right) locomotion

The main lower limb muscles, joints, and segments of the redundant musculoskeletal system manipulated during locomotion are shown. Red and yellow lines indicate one-joint muscles and two-joint muscles, respectively (modified from Aoi and Funato (2016)).

Hence, animals generate the common motor command to coordinate multiple muscles or joint, rather than generating individual movement commands separately. Thus, by acquiring coordination, animals are able to reduce the number of degrees of freedom that need to be controlled. For example, when thigh, shank, and foot elevation angles are plotted against each other, it is known that the angular data covary to form a regular loop (i.e., gait loop) over a plane (Figure 1-2A) (Borghese et al., 1996; Ivanenko et al., 2007). In other words, the three motions of the hip, knee, and ankle joints have intralimb coordination that changes together while maintaining a linear relationship during locomotion. This gait loop feature is found not only in humans but also in other mammals such as cats (Poppele et al., 2002) and monkeys (Figure 1-2B) (Courtine et al., 2005), suggesting that this is a common mechanism inherent in the joint movements that form locomotion.

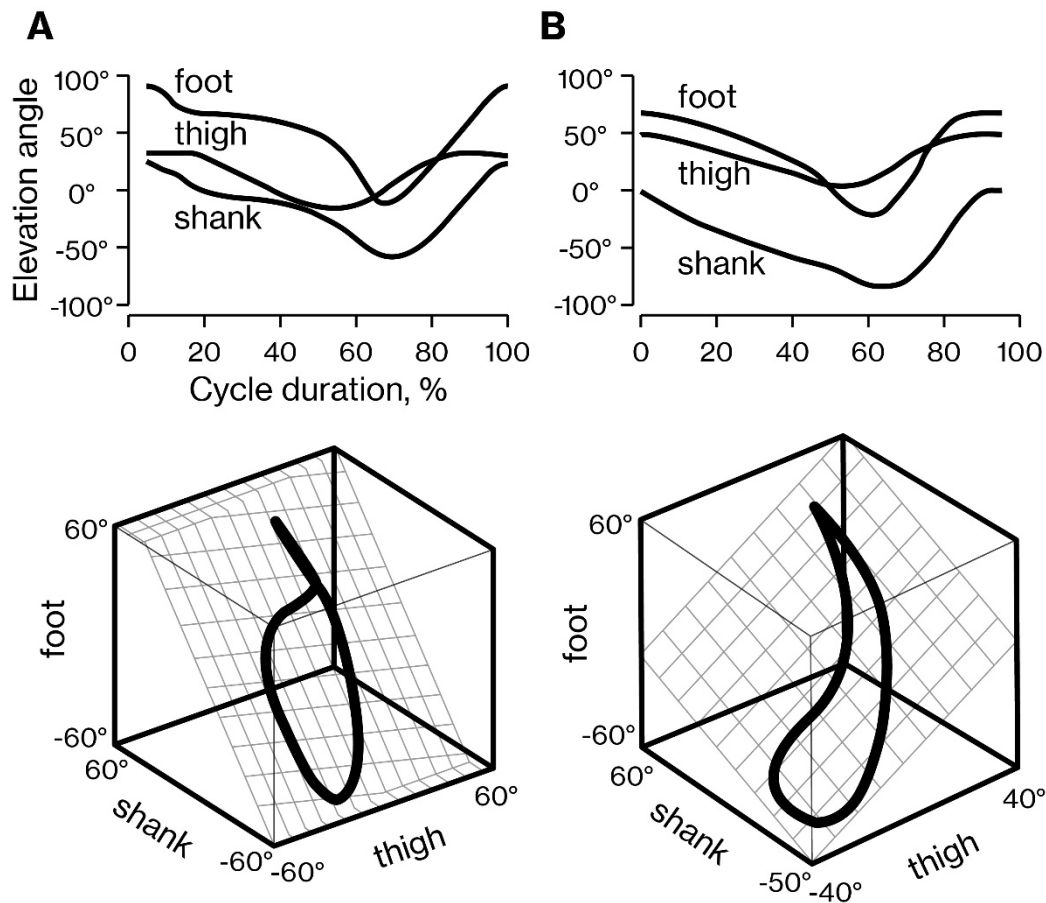


Figure 1-2. Pattern of intersegmental coordination in human (A) and monkey (B)

The waveforms of the thigh, shank, and foot elevation angles are plotted versus the normalized gait cycle (upper). The 3-dimensional (3-D) gait loops obtained by plotting each elevation angle in the upper row versus each other are shown (lower). The grids identify the best-fitting planes. Gait loops progress in time in the counterclockwise direction, the beginnings of the stance phase and the swing phase corresponding approximately to the top and bottom of the loops, respectively (modified from Ivanenko et al. (2007) and Courtine et al. (2005)).

Such cooperative structures are found not only in joint motion but also in muscle activity. From statistical analyses such as principal component analysis (PCA) and non-negative matrix factorization (NMF) of measured electromyographic (EMG) data during

locomotion, despite complicated spatiotemporal properties, muscle activity can be explained by a low dimensional spatiotemporal structure. Ivanenko et al. (2004) examined the EMG data of 25 muscles recorded during human locomotion and reported that they could be explained by a combination of just five basic activation patterns (Figure 1-3).

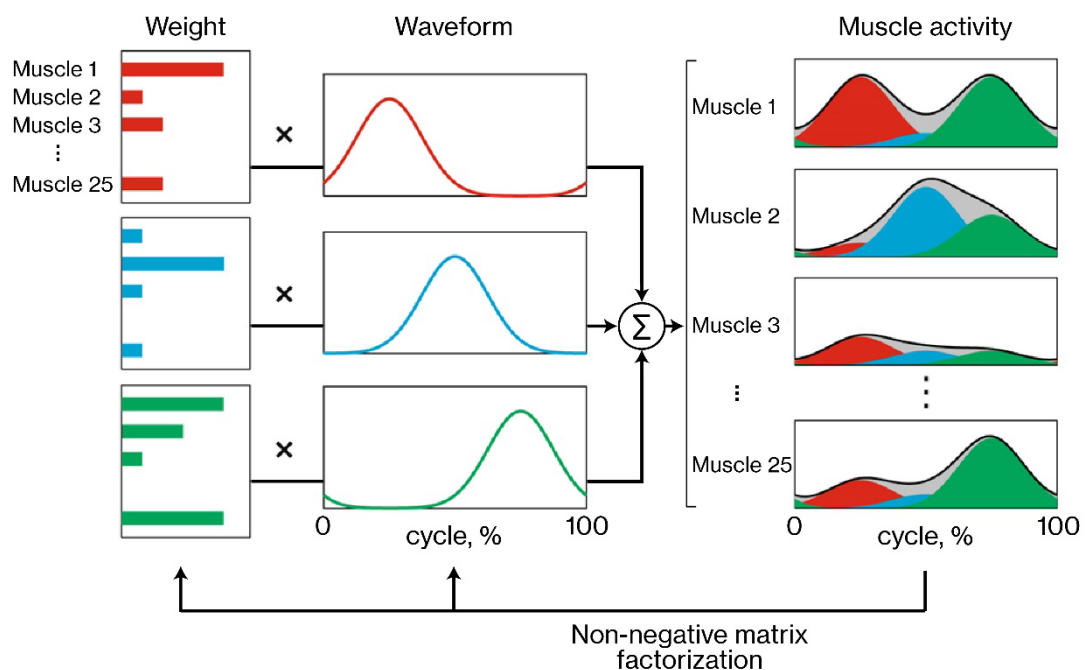


Figure 1-3. Schematic model of basic activation patterns

Basic activation patterns were extracted from muscle activities as weights and waveforms by using NMF. Each weight was represented as an activation balance profile across muscles (muscle 1-25) and activated, through multiplication, by a corresponding waveform. The waveforms resulting from the activations of individual patterns were then summed together to reconstruct the recorded muscle activities (black lines in the right column). More than 90% of muscle activities can be reconstructed by combining five basic activation patterns during human locomotion, but only three of them are shown here to simplify the illustration (modified from Aoi et al. (2019) and Cheung et al. (2012)).

As mentioned above, it has become known that there are cooperative structures in muscle activity (Aoi et al., 2019), joint movement (Stetter et al., 2020), and interlimb coordination (Ivanenko et al., 2007) during locomotion, and therefore many studies have been conducted to search for modular structures that produce coordinated movement in the CNS (Orlovskii et al., 1999). For example, a circuit called the Unit Burst Generator in the spinal cord, which has a structure that binds multiple motor neurons, has been shown by stimulation and impairment experiments on the nervous systems of various animals (Grillner, 1981). On the other hand, little work has been completed on characterizing the modular structures in humans (Ivanenko et al., 2013).

1.2. Altered locomotor patterns in central lesions

CNS lesions may essentially affect central controllers and thus provide some insights into the spatiotemporal organization in patients, which are useful to improve our understanding of modular structures in humans. In particular, if the modular structures are indeed mechanisms that realizes task-level biomechanical goals, then any impairment in the neural control of such modular structures would be expected to result in impaired biomechanical output (Cheung et al., 2009; Clark et al., 2010; Ivanenko et al., 2009). Furthermore, lesion at different level could differentially affect locomotor control. Therefore, examining the locomotor adaptation after damage to different locations, such as the cerebral cortex and spinal cord, will help us to better understand the modular structure.

Many previous studies have suggested that the spinal modular structure plays an important role in generating gait patterns (Aoi and Funato, 2016; Dewolf et al., 2018; Funato et al., 2010; Grasso et al., 2004; Ivanenko et al., 2013). The spinal module interacts

with inputs from the periphery and from descending pathways, and initiate and organize hindlimb locomotion. Therefore, lesion at different level could differentially affect locomotor control. That is, examining the locomotor adaptation after damage to different locations, such as the cerebral cortex, as well as the spinal cord, can help us to better understand the modular structure.

1.2.1. Modular structure in supraspinal injury patients

There are many reports that locomotor deficits after stroke are often associated with abnormal spatiotemporal patterns of muscle coordination (De Quervain et al., 1996; Den Otter et al., 2007; Knutsson and Richards, 1979; Mulroy et al., 2003). Furthermore, it has been suggested that impaired locomotor coordination in post-stroke may be accompanied by not only changes in output pattern of modules, but also by a decrease in the number of modules (Clark et al., 2010; Safavynia et al., 2011). For example, Clark et al. (2010) showed that a less complex muscle coordination pattern in stroke patients. The number of modules in post-stroke patients was reduced, as each module was integrated, which had been observed in healthy subjects (Figure 1-4). This suggests that the independence of neural control signals is reduced. Similar conclusions have been reached in recent studies on upper limb control (Cheung et al., 2009; Cheung et al., 2012). However, in another study, Gizzi et al. (2011) claimed that muscle module numbers are maintained during locomotion in subacute stroke patients. Such discrepancies could be explained by different sets of recorded muscles or by different patient populations.

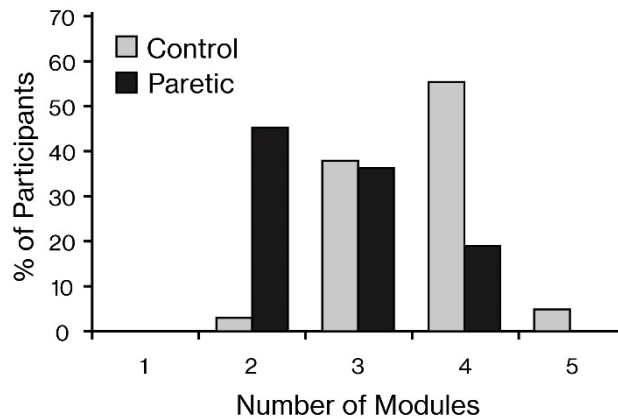


Figure 1-4. Number of modules to reconstruct muscle activity during locomotion

Four modules were needed to reconstruct unilateral lower muscle activity recorded from 8 muscles during locomotion in the majority of healthy control. For the paretic leg of stroke patients, the number of modules required was reduced (modified from Clark et al. (2010)).

1.2.2. Modular structure in spinal cord injury patients

Kinematics analysis has often been used to quantify in detail the gait disturbances in patients with SCI. For example, remarkable differences in the position of the knee and ankle in the sagittal plane were observed between patients with incomplete SCI and healthy subjects (Gil-Agudo et al., 2011). Other reports have suggested injury-induced module changes, such as high gait variability, pronounced flexion posture, and altered distal joint control (Grasso et al., 2004; Lunenburger et al., 2006; McKay et al., 2011). It is also known that intersegmental (thigh, shank, and foot) coordination is impaired in both stroke and SCI, suggesting that this coordination is regulated by the CNS, not a simple consequence of biomechanics (Figure 1-5) (see Chapter 3 in detail).

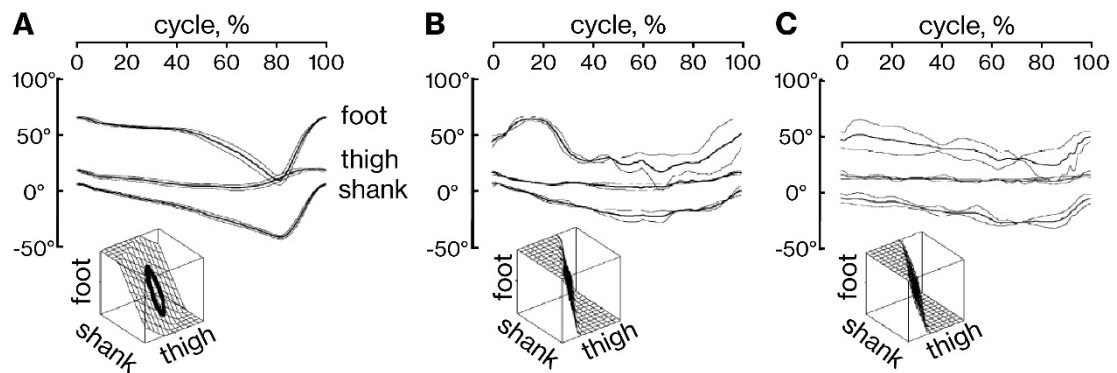


Figure 1-5. Patterns of intersegmental kinematic coordination

The data of healthy subject are shown in A and the data of two SCI patients are shown in B and C. The mean (\pm SD) waveforms of the elevation angles of thigh, shank and foot are plotted versus the normalized gait cycle. The inset in each panel shows corresponding gait loops and best-fitting planes. The planes to the gait loops changed with elevation angles of segments, suggesting that intersegmental coordination was impaired by SCI (modified from Grasso et al. (2004)).

In addition to kinematic analysis, surface EMG can provide additional information on motor control deficits. In a study of gait training with body-weight support in SCI patients, relatively mild patients could regain near-normal kinematics. However, the activation pattern of the muscles used to generate this kinematics was very different from that of healthy subjects (Figure 1-6) (Grasso et al., 2004; Pepin et al., 2003b).

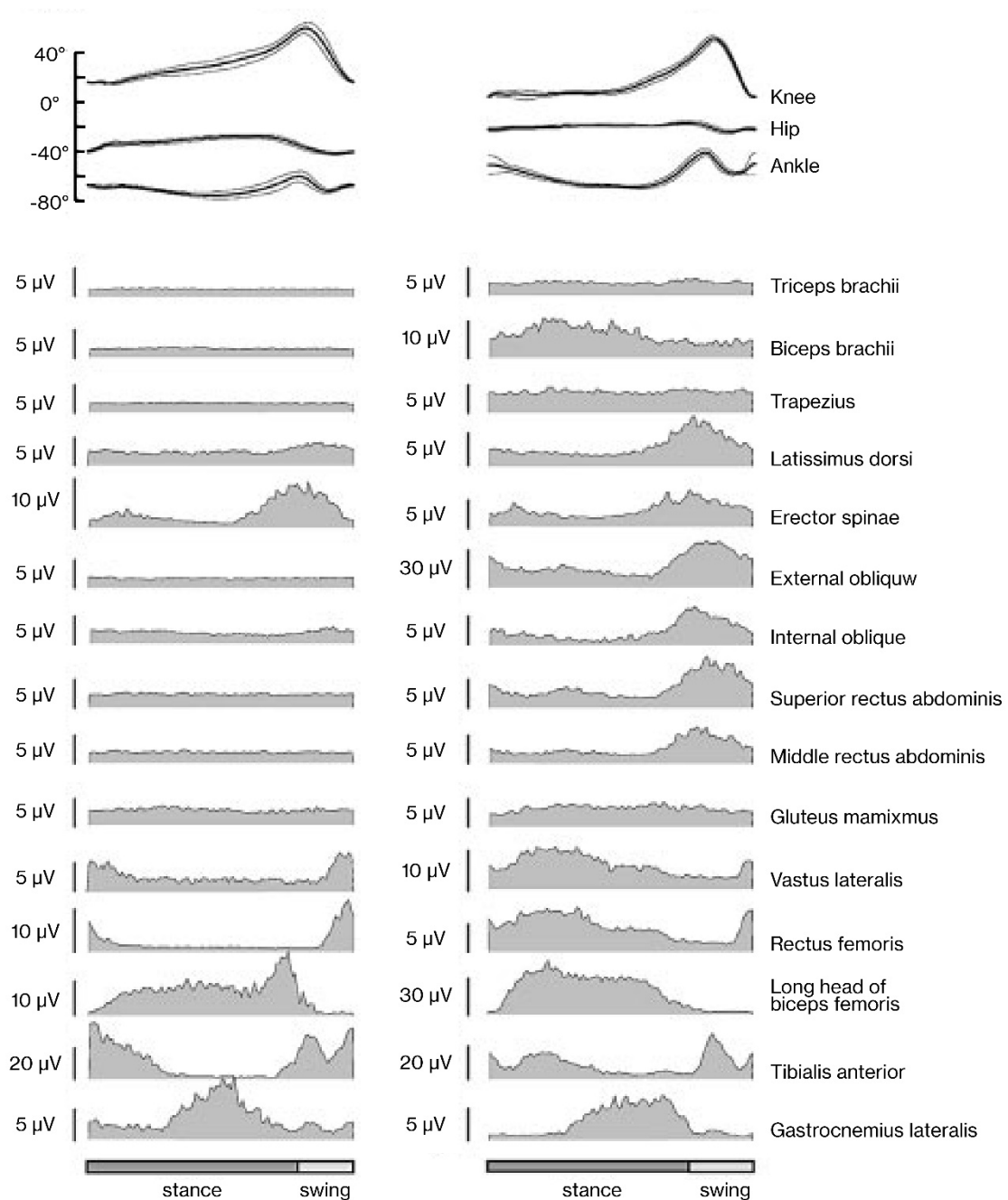


Figure 1-6. Kinematics and surface EMG during locomotion

Joint angles and surface EMG of 15 muscles plotted versus the normalized gait cycle for healthy subjects (left) and gait trained SCI patients (right). Although kinematics of the trained patients was similar to those of healthy subjects, EMG was extremely different (modified from Grasso et al. (2004)).

Thus, human studies have shown that kinematics and muscle activation, which represent as outputs from the CNS, are affected by stroke and SCI and change their patterns. Furthermore, statistical processing of these output patterns suggests that the number of modular structures is reduced or integrated with CNS damage.

1.3. Limitation in human locomotor study

Biomechanical aspects of human locomotion have been documented in many studies in normal gait and pathological gait after SCI. Furthermore, several studies explored the modular structures that generate coordinated kinematics and muscle activation by decomposing them (Bizzi and Cheung, 2013; Davis and Vaughan, 1993; Ivanenko et al., 2006). These findings are discussed in a general context of module structure of the locomotor program and compensatory gait mechanisms and are helpful to the development of improved rehabilitation strategies (Ivanenko et al., 2013).

However, human SCI studies are limited in their ability to improve our understanding of modular structures for locomotion for the following reasons. First, detailed human spinal cord pathology cannot be inferred in clinical trials. In human SCI, multiple pathways are severed simultaneously by an external force. Therefore, the spared descending pathways from the supraspinal structures play an active role for locomotion. Figure 1-7 summarizes the location of the main descending pathways in the mouse spinal cord (Holstege and Kuypers, 1987; Petras, 1967; Rossignol and Frigon, 2011) that may be damaged after SCI. For example, pontine reticulospinal and vestibulospinal pathways located at ventral side may be critical in initiating locomotion and postural control (Jordan, 1991). Corticospinal and rubrospinal pathways located at dorsal side are important for volitional and goal-directed aspects of locomotion, as well as fine control of the distal

musculature (Liddell and Phillips, 1944). Although techniques to detect the lesion extent by conventional magnetic resonance imaging (MRI) and the fiber tract by diffusion tensor imaging (DTI) have been developed, the resolution of these techniques may be insufficient to assess some trauma-induced changes in vivo (Freund et al., 2019). Besides, many of these studies compare clinical, functional scores with locomotor kinematics, and it is unclear how they reflect the actual pathology. Furthermore, in human SCI studies, it is difficult to compare neuropathology and gait output patterns under the same conditions (facility, location of injury, and time onset after SCI). To overcome these limitations, cross-sectional studies in animal models to compare neuropathology and locomotor patterns will help to complement these findings.

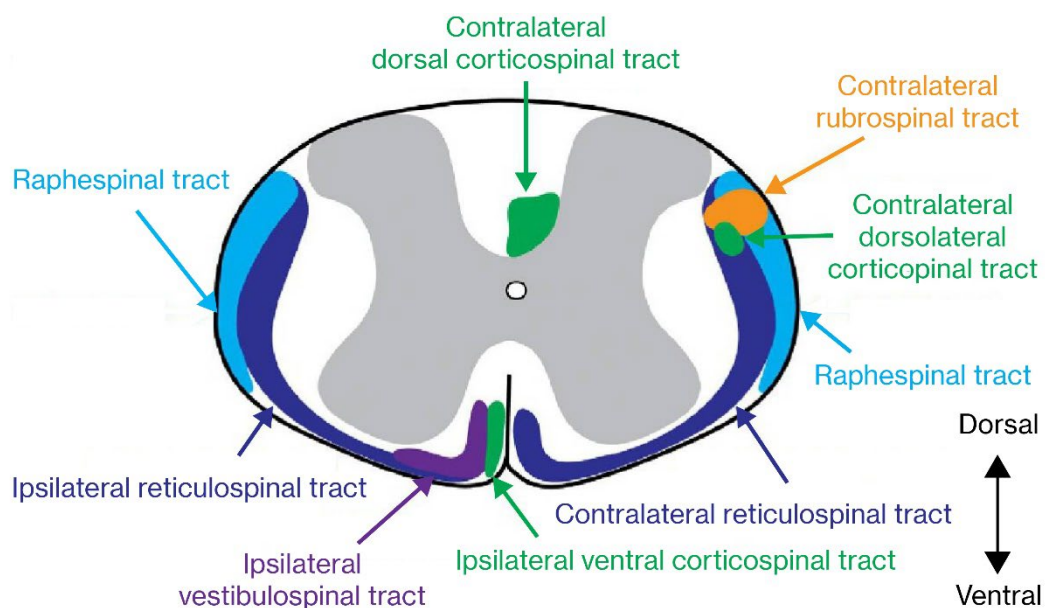


Figure 1-7. Descending pathways in the spinal cord of a mouse

Schematic representation of the main descending tracts in a coronal section of the spinal cord in a mouse. Each color indicates the location of a pathway that projects from an anatomically different region to the spinal cord (Modified from Roussel et al. (2020)).

Second, since most human SCI is caused by accidents or falls, individual differences in the location and extent of injury occur, resulting in different neuroplasticity and behavioral changes. There is a growing consensus that recovery largely depends on plasticity phenomena induced by the lesion, such as modified synaptic strengths and sprouting of spared pathways (Figure 1-8) (Barbeau et al., 1999; Calancie et al., 2002; Calancie et al., 1994; Dobkin, 2000; Harkema et al., 1997; Raineteau and Schwab, 2001; Wernig et al., 1995). Therefore, different damages could induce different changes in the module structure. Indeed, experimental studies performed on SCI patients have demonstrated distinct adaptations (Goldberg and Neptune, 2007; Grasso et al., 2004; Ivanenko et al., 2009). Therefore, to define the relationship between the plasticity of the modular structure and the output gait pattern after SCI, longitudinal studies under the same conditions such as partial transection (hemisection) model using animal experiments are becoming more critical.

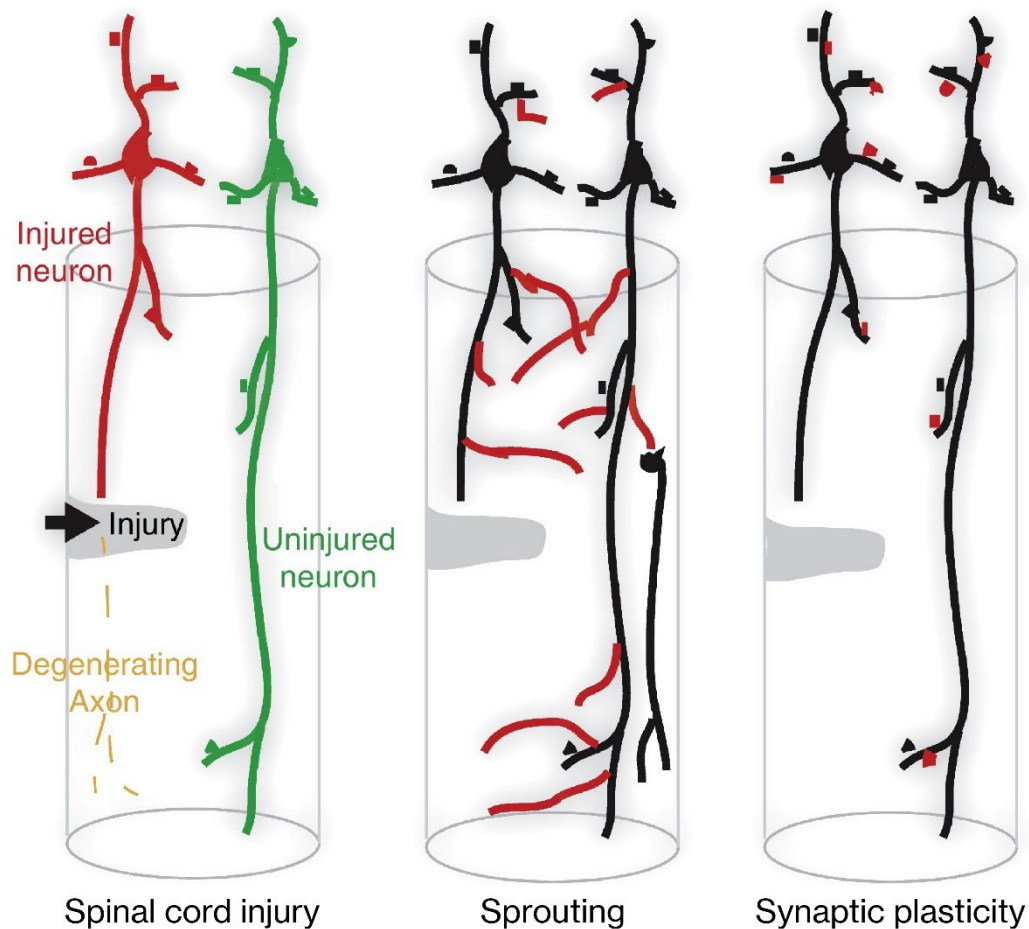


Figure 1-8. Plasticity phenomena induced by SCI

Injuries to the CNS of traumatic etiology typically damage certain axonal pathways but spare parallel pathways (left). Recovery and repair can be supported by plasticity phenomena. Uninjured and injured fibers that are rostral and caudal to the injury can sprout to form new connections (middle), or plastic changes of presynaptic and postsynaptic connections throughout the nervous system (right) (modified from Schwab and Strittmatter (2014)).

1.4. Difference in rodent, non-human primate, and human for locomotion after SCI

Although human studies have limitations and need to be validated by studies using animal models, it may be difficult to directly apply the results in animal models to humans. For example, several promising of therapies have been developed in rodents to restore gait

function and reached the clinical trial stage, but outcomes often fall short of expectations (Cote et al., 2017). This discrepancy may be due to differences in the mechanisms of gait control between rodents and humans. So far, a common gait control system across species has been described, but the differences between them need to be considered. In particular, differences in the dependence on supraspinal input after injury may be an important factor. Despite the smaller size of CNS in rodents, their spinal cord accounts for 30% of the CNS weight, compared to only 3% in humans (Swanson, 1995). Overall, the spinal cord in rodents may actually have more computing power than in humans. Furthermore, locomotor training improves the recovery of stepping movements in mice (Fong et al., 2005) and rat model (Cha et al., 2007; Timoszyk et al., 2005) after complete transections, but motor complete SCI patients, despite similarly intensive treadmill training (Dietz et al., 2002). On the other hand, it has been suggested that primates may be more similar to humans than rats in the degree of recovery of motor gait function in cervical hemisection model (Friedli et al., 2015). Inconsistencies in results obtained between rodents and non-human primates or humans suggest that it is more beneficial to conduct studies in non-human primates, bridging the gap in knowledge between them. Overall, when considering human applications, it may be necessary to verify whether the concept of gait control validated in rodents is also valid in primates.

1.5. Purpose of the Dissertation

In this dissertation, the author examined the relationship between locomotor output pattern and neuropathology by using the SCI animal models in order to discuss the underlying modular structure.

A large number of kinematic data were needed for studies of animal locomotion,

and traditional kinematic analyses using reflective markers attached on animals' skin have been used for evaluating locomotor deficits; however, this marker-based approach has some issues to consider in both recording and analysis. The attached markers are potentially distracting to animals (Perez-Escudero et al., 2014), and the marker positions are often manually digitized afterward, which is a labor-intensive and time-consuming procedure. These situations constrain the number of groups, animals, and evaluations that can be included within the experimental plan. Therefore, the author adapted the motion capture method using deep learning to analyze the locomotion of SCI animals and demonstrated that the method could accurately evaluate locomotor deficits caused by SCI (Figure 1-9) (Sato et al., in Press-b). This made it possible to analyze a large number of samples.

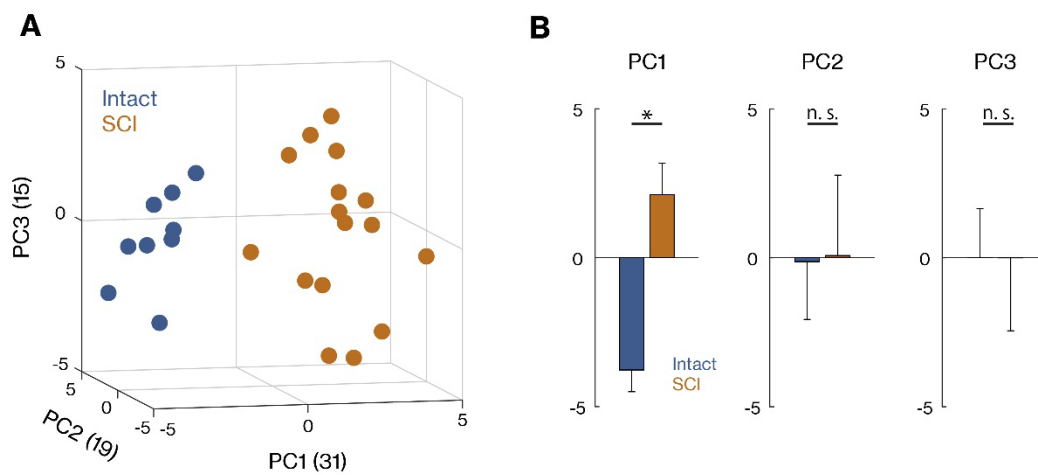


Figure 1-9. Deep learning based kinematics in intact and SCI mice

PCA was applied to 30 kinematic parameters, which were quantified by using a trained deep neural network distinguished gait patterns underlying locomotion between intact (blue dots, n = 9) and SCI (orange dots, n = 16) mice (A). The principal component 1 (PC1) scores were significantly different between intact and SCI mice. * $p < 0.001$; ns, not significant, Welch's t -test (B) (modified from Sato

et al. (in Press-b)).

By using these deep learning based kinematics, the author has demonstrated cross-sectional analysis of a large number of SCI mice and longitudinal analysis of marmosets with a uniform degree of damage due to partial transection. In Chapter 2, the author examined the differences in locomotor output patterns cross-sectionally in SCI mice with varying degrees of injury and tested whether there was a relationship between neuropathology and compensatory locomotor patterns. However, it is known that not only locomotor diversity depends on the degree of damage but also that there is a plastic change over time after injury in the modular structure (Ivanenko et al., 2003). Therefore, in Chapter 3, the author examined the plastic change of intersegmental coordination by assessing the gait loops longitudinally in marmosets with the same degree of damage and tested how the locomotor output changed over time after SCI. Finally, in Chapter 4, the author expresses a perspective on the contribution of this dissertation to the scientific and technological breakthroughs in the field of neurofeedback by summarizing the findings of the two aforementioned studies.

Chapter 2: Functional reorganization of locomotor kinematic synergies reflects the neuropathology in a mouse model of spinal cord injury

*This chapter was based on the following author's original article:

“Sato, Y., Kondo, T., Shibata, R., Nakamura, M., Okano, H., Ushiba, J., in Press-a. Functional reorganization of locomotor kinematic synergies reflects the neuropathology in a mouse model of spinal cord injury. *Neuroscience Research*” The author has a right to use this dissertation.

2.1. Introduction

SCI disrupts communication between supraspinal centers and lumbosacral spinal circuits, causing a range of walking disabilities. Patients with SCI generally have some preservation of walking ability (Squair et al., 2021). However, they rarely achieve a similar level of gait function as unaffected people and have approximately twice the risk of falling as healthy older people (Brotherton et al., 2007). Thus, although there may be different gait control system in SCI patients than in healthy individuals (Rossignol and Frigon, 2011), these are not yet well understood.

Humans and animals engage in adaptive walking by controlling redundant musculoskeletal system composed of numerous muscles and mechanical degrees of freedom. Previous physiological studies in humans and animals have shown that the CNS organizes these redundant systems by generating the common motor command to coordinate multiple muscles or joints (Aoi and Funato, 2016; Bizzi et al., 1991; Cappellini et al., 2006; Grillner, 1981; Ivanenko et al., 2008; Latash, 1999). This coordinated pattern

of muscle activities or joint angle movements can be extracted as common components using dimensionality reduction techniques, such as PCA (Catavittello et al., 2018; Courtine et al., 2005; Stetter et al., 2020) or NMF (Cheung et al., 2012; Chvatal et al., 2011; Clark et al., 2010; Martino et al., 2019).

To characterize kinematic coordination patterns, PCA is performed on a kinematic data set and decomposes a complex kinematic pattern into main kinematic synergies (Daffertshofer et al., 2004; Lamoth et al., 2009; Stetter et al., 2020; Wang et al., 2013). For example, previous studies of multisegmental coordination during walking using PCA revealed that the first 3-5 components are sufficient to describe the walking pattern's major features (Courtine and Schieppati, 2004; Daffertshofer et al., 2004; Lamoth et al., 2009; Wang et al., 2013). An investigation of the basic coordination patterns for different locomotor tasks showed that invariant coordination patterns were found while performing different tasks such as straight-line walking and walking turns (Courtine and Schieppati, 2004), or walking and running (Lamoth et al., 2009). Furthermore, turn-dependent coordination pattern adjustments were observed depending on the turn direction (Courtine and Schieppati, 2004). Conversely, patients with SCI can only adjust speed within a limited range and cannot increase stride length (Pepin et al., 2003a), which may reflect disorder in the modular structure that generates the kinematic coordination pattern. However, it is unclear whether the original coordination patterns are preserved, or new coordination patterns are acquired, and whether these compensatory gait strategies depend on their pathophysiological background.

Therefore, the main objective of the study in this chapter is to investigate SCI-induced changes in kinematic synergies. For this purpose, the author recorded kinematic data from intact and SCI mice walking on a treadmill. the author then applied PCA to

extract kinematic synergies from the integrated data. Next, the author classified the kinematic synergies of SCI mice by applying a hierarchical cluster analysis on the extracted synergy components. Finally, the degree of spared tissue at the lesion epicenter of the spinal cord in each group was compared to verify if the differences in kinematic synergies reflect the underlying SCI neuropathology.

2.2. Material and Methods

2.2.1. Animals

The current study used female C57B16/J mice (8 weeks old, 18-20 g, n = 30) because bladder expression is easier, and complication risk is reduced compared with male mice. The animals were housed in a 12:12h light/dark photoperiod and food and water were available ad libitum. All the animal procedures were approved by the ethics committee of Keio University (Number: 13020) and were conducted according to the guidelines of the National Institutes of Health.

2.2.2. Experimental procedure

Mice were anesthetized by intramuscular injection of ketamine (100 mg/kg) and xylazine (10 mg/kg). The skin over the back was shaved and disinfected with 70% alcohol. Skin and superficial back muscle were cut and retracted from each side between T8–T12. Then, laminectomy was performed between T9–T11, and spinal contusion injuries were produced at T10 using an Infinite Horizon impactor (Precision Systems and Instrumentation, Fairfax Station, VA) with 70 kdyn. All efforts were made to minimize animal suffering.

2.2.3. Kinematics Recording

Mice were briefly anesthetized with isoflurane to estimate the centers of rotation of the joints through palpation on the skin. The shaved skin at the iliac crest, the hip joint, the knee joint, the ankle joint, the metatarsophalangeal (MTP) joint, and the tip of the fourth toe were marked with a black permanent marker pen. The mice were put in a Plexiglas enclosure (320×160×40 mm) placed over the treadmill belt. GoPro (GoPro, Inc., CA) (240 frames/s, 1,280×960 pixels), placed on the left side at approximately 120 mm from the treadmill, was used to record the mice walking on the treadmill for ~10 min per mouse. Since impairments with lateral movements, such as a circumduction gait, are rarely apparent after the injury with the severity used here, the walking was recorded in the sagittal plane (Alluin et al., 2011; Leblond et al., 2003). Indeed, the walking was visually observed while recording and confirmed that such impaired gait was not generated. Since the GoPro is equipped with a fisheye lens that causes image distortion, “Lens Distortion” (curvature = -31) was applied to the recorded videos in Premiere Pro (Adobe, Inc., CA). To determine the treadmill speeds which allow them to control cyclic gait, they were placed on the treadmill set at a speed of 3–20 cm/s (in 1 cm/s steps). The treadmill speeds were decided 10 and 15 cm/s in intact mice and 7 cm/s in SCI mice. Gait at 10 cm/s and 15 cm/s in intact was used to see if the treadmill speed would alter the synergies. The analyzed walking cycles were manually selected based on previous studies (DiGiovanna et al., 2016; Fiander et al., 2017). The trials during which the mouse walked at least three consecutive steps were included without the first and last steps. Additionally, any steps other than walking, such as jumping and running, were excluded. The inclusion number per mouse was 16 ± 3 cycles (mean \pm SD).

Each joint was tracked using Deeplabcut, a markerless pose estimation system

based on transfer learning with deep neural network (Mathis et al., 2018). The standard DeepLabCut workflow was followed. In 1,000 training frames randomly sampled across all mice in each of intact and SCI, and all parts were manually labeled. Thereafter, the deep neural network was trained using 90% of the labeled images as training and 10% as testing. Training proceeded for 300,000 iterations to reach cross-entropy loss plateau. The NVIDIA GeForce RTX 2070 Graphics Card was used for training. The neural network performance was measured by computing the root-mean-squared error between the manual labels and those predicted by DeepLabCut.

2.2.4. Kinematic synergy extraction

MATLAB 2020a (MathWorks, Inc., MA) was used for data processing and synergy extraction. Since the joints were not tracked using Deeplabcut correctly in a certain number of frames, x- and y-coordinates were filled using linear interpolation (< 1% of the data). The cycle duration multiplied by the treadmill speed was added to x-coordinate of each body part to facilitate comparison of walking between different treadmill speeds. Each walking cycle was defined as a foot contact to the next foot contact and subdivided into the stance and swing phase by foot lift. The timing of the foot contact and foot lift was determined visually from the videos. All coordinates of each stance and swing phases were time-normalized, such that the duration of each phase was represented by 50 frames, and spatially normalized, such that each mean was 0 and each standard deviation (SD) was 1. Based on the processed data, a coordinate data set was formed for each analysis, in which all cycles in all mice to analyze were concatenated into one matrix. Therefore, the dimension of the matrices was all frames analyzed (total number of trials to analyze \times 100 frames) \times 12 (6 joints \times 2D coordinates). In intact mice, the median values of

between-individual and within-individual correlation were compared using Mann-Whitney U test to verify if it was justified to concatenate all mice data. In SCI mice, the concatenated data were made for each mouse to identify the mouse-specific synergies.

Kinematic synergies consisting of spatial and temporal components were extracted from concatenated data as described above using PCA (Daffertshofer et al., 2004; Lamoth et al., 2009; Stetter et al., 2020; Wang et al., 2013). PCA returned eigenvectors, scores, and eigenvalues. Eigenvectors formed the basis of a coordinate system, known as spatial component W_k , where k denotes the order of the principal component (PC). Moreover, W_k in intact and SCI mice were referred to as $W_{\text{intact},k}$ and $W_{\text{SCI},k}$, respectively. $W_{\text{SCI},k}$ was extracted from each SCI mouse, and reversed (the sign of the loading was changed) whenever necessary so that they had the same orientation as $W_{\text{intact},k}$ (positive dot products of $W_{\text{intact},k}$ and $W_{\text{SCI},k}$). Scores obtained by projecting the data onto each W_k are time series that describe the temporal information of a corresponding PC; they are known as temporal component S_k . The eigenvalues quantify the variance of each PC.

Parallel Analysis (PA) was used to determinate the number of components to retain in intact mice (Franklin et al., 1995). In this procedure, eigenvalues from the data to be applied to PCA were compared with those from a matrix of random values (mean of 0, SD of 1) of the same dimensionality. The PCs of which eigenvalues were greater than PA eigenvalues were retained.

For an intuitive interpretation of the synergies, principal movements were identified by the corresponding PC_k in intact mice:

$$M_k = P_0 + \sigma S_k W_k$$

where M_k represents each joint position of each principal movement. P_0 is a row vector

denoting the average posture, calculated as the mean of the concatenated data. σ is also a row vector and calculated as SD of each coordinate from the concatenated data before spatial normalized. The coordinates denoted by M_k were drawn continuously as stick pictures frame by frame to identify the principal movement visually.

2.2.5. Hierarchical clustering

To group the individual-specific synergies, a cluster analysis was applied based on the spatial components (Gracia-Ibanez et al., 2020). Since a hierarchical cluster analysis (grouping metric: cosine; method: complete) was used, it considers similarity through the angle between each eigenvector. The groups were formed in an agglomerative manner, starting with each observation as their own group and at every step pairing the two closest groups together until only one group remains. The number of subgroups was chosen based on visual inspection of the dendrograms. The concatenated data were made for each group from all mice include in each group, and PCA was applied to each data to identify group-specific synergies categorized by the hierarchical cluster analysis. The eigenvectors extracted from each group were referred to $W_{Gg,k}$, where g denotes each group number.

2.2.6. Similarity analysis

To quantify the similarity of synergies in each group with those in intact mice according to spatial components, each $W_{Gg,k}$ was modeled as a linear combination of $W_{intact,k}$:

$$W_{Gg,i} \approx \sum_{k=1}^{12} m_k W_{intact,k}, i = 1, 2, 3$$

where m_k is a coefficient denoting the degree of contribution of $W_{intact,k}$ to the structure of the i th $W_{Gg,i}$ in the liner combination. The more similar $W_{Gg,k}$ are to $W_{intact,k}$, the larger the

absolute value of the same order coefficient (e.g., m_1 for $k = 1$ or m_2 for $k = 2$), which is 1 if they are the same.

2.2.7. Tissue processing and analysis

All mice were anaesthetized by intramuscular injection of ketamine (100 mg/kg) and xylazine (10 mg/kg) and perfused with PBS (5 ml) and 4% paraformaldehyde (5 ml) at 30–31 days after SCI. Spinal cords containing the lesion area were dissected and post-fixed in 4% PFA for 24 h before being cryoprotected in 30% sucrose for 48 h. Serial transverse sections (20 μ m) were cut through the lesion area on a cryostat (Leica CM3050 S), and every 5th section was collected and stained using hematoxylin and eosin. The section with the largest extent of the lesion was designated the epicenter. Sparing tissue was quantified and represented as a proportion to total area of the spinal cord at the lesion epicenter using ImageJ software version 1.53c (Ito et al., 2018; Tashiro et al., 2016). To verify the assumption for the homoscedasticity, Bartlett's test was applied. After confirming that Bartlett's test resulted to be not significant, the degree of sparing tissue was compared between the groups by one-way ANOVA followed by Tukey *post-hoc* comparison.

2.3. Results

2.3.1. Kinematic synergies in intact mice

The author recorded intact mice walking on the treadmill (7 mice: a total of 104 trials) and applied signal processing in x- and y-coordinates of each joint tracked using Deeplabcut (Figure 2-1A). Each walking cycle was subdivided into the stance and swing phases, followed by temporal and spatial normalization. To test if it was justified to

concatenate all mice data, the author compared the between-individual correlation to within-individual correlation. The median values of between-individual and within-individual correlation were 0.909 [0.850–0.917] (Median [1st quartile–3rd quartile]; n = 21, all combinations of 7 mice) and 0.927 [0.909–0.942] (n = 7), respectively, and a significant difference was not observed (p = 0.113; Mann-Whitney U test). Therefore, the author considered that the walking pattern was equivalent among mice. All cycle data recorded in intact mice was concatenated into a matrix to which the PCA was applied.

The PCA eigenvalues from the data and PA eigenvalues from the corresponding randomized data are reported in Figure 2-1B. The author applied PA to a matrix of the same dimension as the data (10400 × 12) to determinate the number of components to retain. As a result, first three PCA eigenvalues were greater than PA eigenvalues.

The spatial components $W_{\text{intact},1-3}$ and the corresponding temporal components $S_{\text{intact},1-3}$ extracted by intact mice data are illustrated in Figure 2-1C (left and middle, respectively). Moreover, based on these components, the author identified the corresponding principal movement (Figure 2-1C, right). PC₁, since the temporal component increases throughout the cycle, was represented unidirectional forward propagation (not backward). In PC₂, which represented forward-bent/backward-bent, the temporal component increases from the beginning of the cycle to the early swing phase, and conversely, decreases from the early swing phase to the end of the cycle. PC₃, which represented upward/backward movement, shows a negative peak in the middle of each of the stance and swing phase. Moreover, to see how kinematic synergies changed in response to environmental changes, the author compared the spatial components in mice walking between different treadmill speed. The dot products of spatial components in 10 cm/s and 15 cm/s of the same PC were large (PC₁, 0.98; PC₂, 0.95; PC₃, 0.94), suggesting

that these synergies were independent of walking speed.

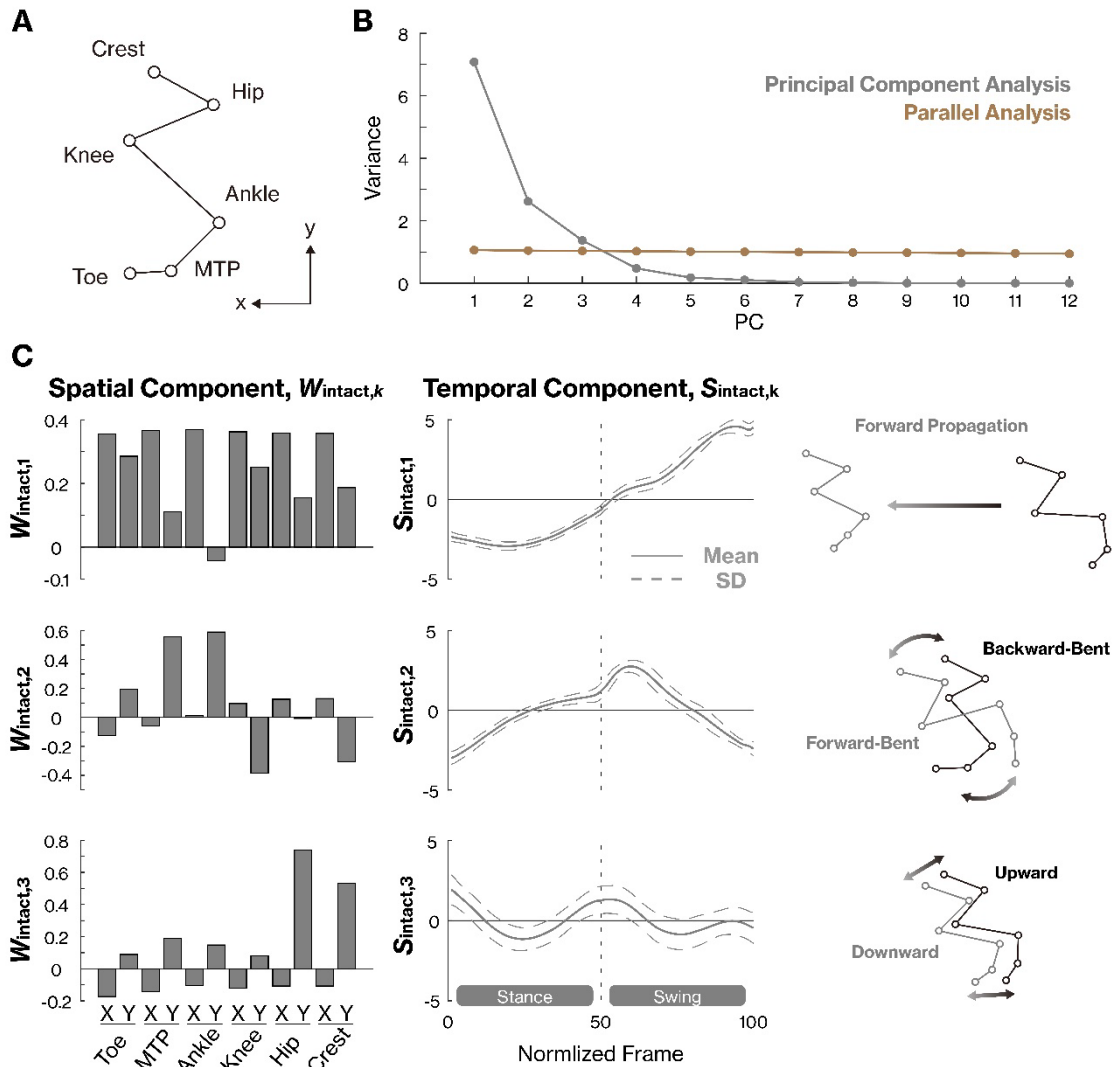


Figure 2-1. Kinematic synergies in intact mice

(A) Coordinates of the six points used to construct a stick model of the hindlimb; Crest, hip, knee, ankle, MTP, and toe.

(B) The eigenvalues calculated using each of principal component analysis (gray) and parallel analysis (brawn). The PCA eigenvalues were calculated from the concatenated data set covering all cycles recorded in intact mice. Note that the PA eigenvalues were almost one because the matrix used for PA was large (dimension, 10400×12). First three PCA eigenvalues were greater than PA eigenvalues.

(C) The spatial components $W_{\text{intact},1-3}$ (left), the temporal components $S_{\text{intact},1-3}$ (middle), and the stick models representing principal movement (right) corresponding each PC. The bars in spatial components indicate the weightings of x- and y-coordinates of each joint. Each temporal components shows mean \pm SD. The dashed vertical lines indicate the time to switch the phase, this is, first half and second half are stance and swing phase, respectively. The principal movements were calculated based on W_k and S_k , and show the movement in the direction indicated by the arrow during each cycle.

2.3.2. Kinematic synergies in SCI mice

All the mice showed flaccid paralysis of the hindlimbs immediately after the SCI. 17 mice were able to walk stably over the treadmill belt and were recorded. Equivalent walking patterns in intact mice enabled to concatenate all data, however, those in SCI mice were different from one another. Therefore, PCA was applied to the processed data of each mouse to identify the mouse-specific synergies, i.e., the author performed PCA 17 times in total during this procedure. To investigate SCI-induced synergy change, the author compared the characteristics of first three spatial components among SCI mice. $W_{\text{SCI},1}$ were similar among all SCI mice, and represent almost the same spatial components to intact mice. However, the characteristics of $W_{\text{SCI},2}$ and $W_{\text{SCI},3}$ differed from a mouse to another. Therefore, the author applied a hierarchical cluster analysis to each of $W_{\text{SCI},2}$ and $W_{\text{SCI},3}$. Based on each dendrogram, the author identified the number of groups in $W_{\text{SCI},2}$ (Figure 2-2A upper) was three, and it was also three in $W_{\text{SCI},3}$ (Figure 2-2A lower). Interestingly, although the author applied this cluster analysis for $W_{\text{SCI},2}$ and $W_{\text{SCI},3}$, respectively, the individuals included each group were the same for $W_{\text{SCI},2}$ and $W_{\text{SCI},3}$ (6 individuals in group 1; 7 individuals in group 2; 4 individuals in group 3). Therefore, the author applied PCA to the concatenated data of all individuals included in each group to

identify group-specific synergies. The $W_{Gg,1-3}$ in each group are illustrated in Figure 2-2B. $W_{Gg,1}$ were similar to $W_{intact,1}$ in all groups, while $W_{Gg,2}$ and $W_{Gg,3}$ showed different characteristics in group 2 and 3. In intact and group 1, W_2 consisted mainly of the y-coordinates of MTP, Ankle, and Knee, and W_3 consisted mainly of the y-coordinates of Hip and Crest (Figure 2-1C left, Figure 2-2B left), but in group 2 and 3, these components were not separated in W_2 and W_3 , but were present in both (Figure 2-2B middle, right).

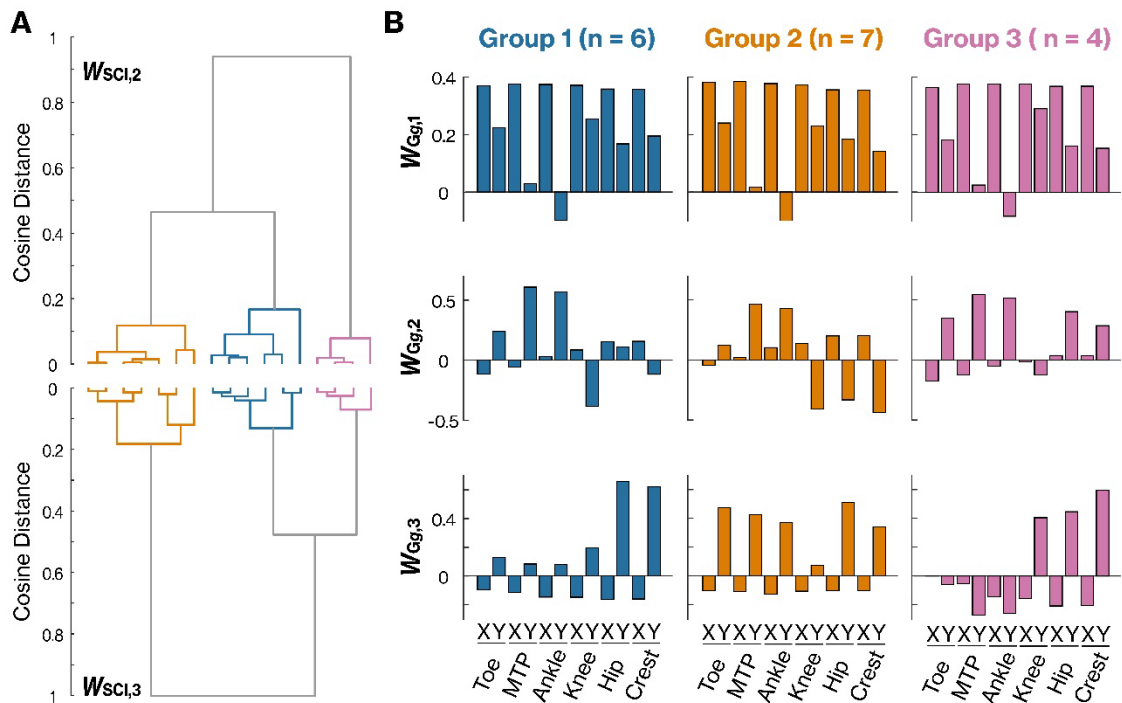


Figure 2-2. Kinematic synergies in SCI mice, grouped into three groups

(A) Dendrograms based on each of $W_{SCI,2}$ (upper) and $W_{SCI,3}$ (lower). Distance on the y-axis and $W_{SCI,2}$ or $W_{SCI,3}$ on the x-axis. The distances were calculated as cosine. The number of groups was set to three based on each dendrogram, and they are identified by color (blue, group 1, $n = 6$; orange, group 2, $n = 7$; purple, group 3, $n = 4$).

(B) W_{1-3} extracted from the concatenated data in each group. The group colors correspond to those in dendrogram. $W_{Gg,1}$ were similar to $W_{intact,1}$ (shown in Figure 2-1C) in all groups, while $W_{Gg,2}$ and

$W_{Gg,3}$ showed different characteristics in group 2 and 3.

To quantify the changes of these synergies from intact according to their W_k , vector composition was performed by modeling each $W_{Gg,i}$ as a linear combination of the set of $W_{\text{intact},k}$. In group 1, the same order coefficients m_k were high in each of $W_{G1,1-3}$ (> 0.97) (Figure 2-3 upper) and the different order coefficients were low (< 0.2), suggesting that almost the same synergies were extracted as intact. While in group 2, although m_1 was higher in $W_{G2,1}$, m_2 was lower and m_3 was higher in $W_{G2,2}$, and m_3 was lower and m_2 and m_4 were higher in $W_{G2,3}$. Similarly in group 3, m_3 was higher than m_2 in $W_{G3,2}$, and m_2 was higher than m_3 in $W_{G3,3}$. These results suggest that the spatial components were intermingled in group 2 and 3, and as a result, the synergies were different from that of intact mice.

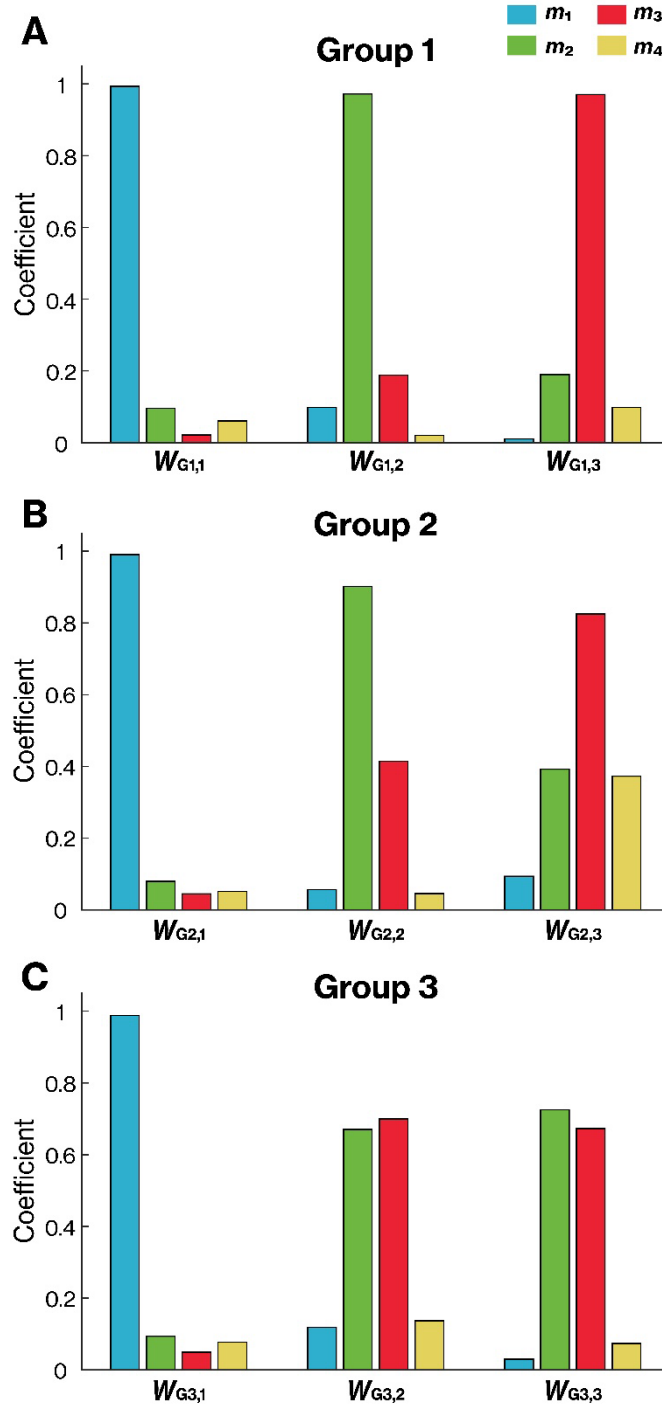


Figure 2-3. The absolute values of coefficient calculated as a liner combination

(A) The coefficient in group 1. $W_{G1,1}$, $W_{G1,2}$, and $W_{G1,3}$ are shown from the left, each with four bars representing m_{1-4} because the coefficients of higher order than m_4 were small in most cases

(Supplementally Table 1). All of m_1 (blue) of $W_{G1,1}$, m_2 (green) of $W_{G1,2}$, and m_3 (red) of $W_{G1,3}$ were approximately 1, indicating that spatial components in group 1 were similar to intact.

(B) The coefficient in group 2. Conventions are the same as in A. As in group 1, m_1 of $W_{G2,1}$ was approximately 1. In contrast, m_2 of $W_{G2,2}$ and m_3 of $W_{G2,3}$ were small and m_3 of $W_{G2,2}$ and m_2 of $W_{G2,3}$ were large, indicating that spatial components were intermingled in $W_{G2,2}$ and $W_{G2,3}$.

(C) The coefficient in group 3. Conventions are the same as in A. As in group 1 and 2, m_1 of $W_{G3,1}$ was approximately 1. In $W_{G3,2}$ and $W_{G3,3}$, m_3 was higher than m_2 and m_2 was higher than m_3 , respectively, indicating that spatial components were intermingled more in $W_{G2,2}$ and $W_{G2,3}$ than in group 2.

Since the spatial components extracted from group 1 were similar to those from intact mice, the author investigated if the walking impairment appeared in temporal components. Thus, the author applied PCA to the concatenated data of intact and group 1 to compare the temporal components obtained by projecting the data onto the same spatial components. The S_{1-3} in each group are illustrated in Figure 2-4. A characteristic difference was not identified in S_1 . In S_2 of group 1, sharply positive peak in early swing which was observed in intact disappeared. In S_3 of group 1, negative peaks observed in the mid-stance and mid-swing disappeared. These results indicated that the temporal components changed in group 1, in which the spatial components were similar to intact mice.

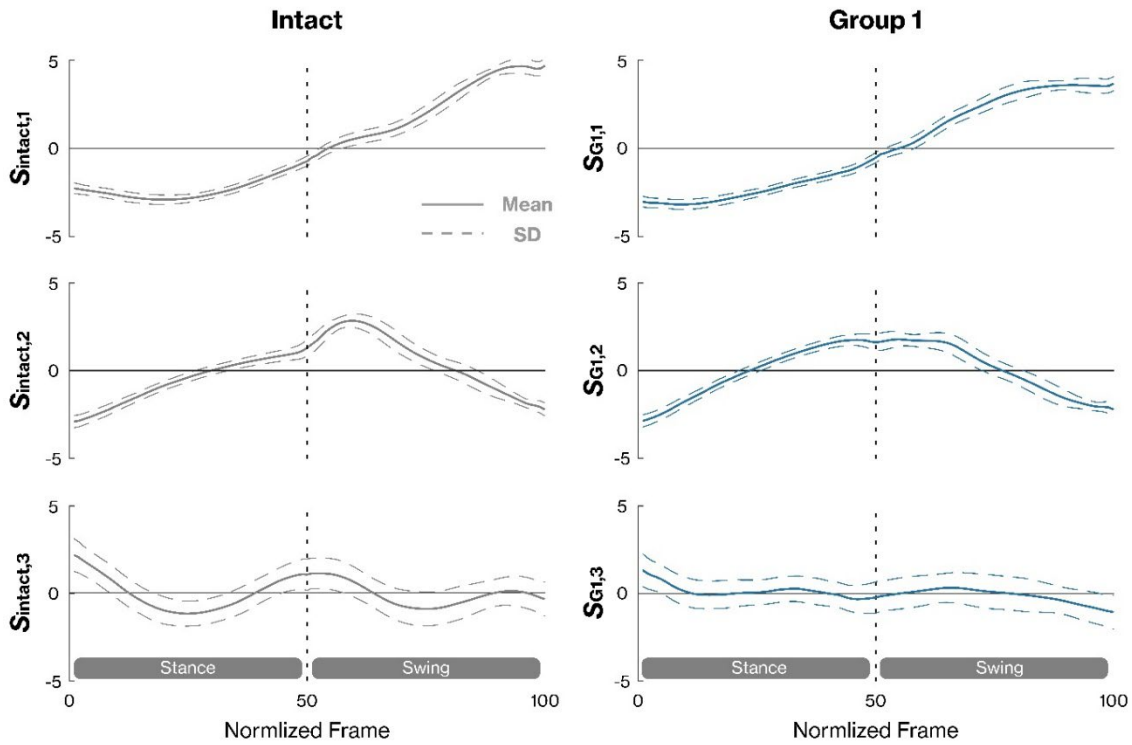


Figure 2-4. The scores in intact mice and group 1

The temporal components S_{1-3} (mean \pm SD) in intact mice (left) and group 1 (right). Conventions are the same as in Figure 2-1C. No characteristic differences were observed between S_1 of intact mice and group1, while S_2 and S_3 showed different characteristics in the waveforms.

2.3.3. Morphometric analysis of SCI

To investigate if these differences in kinematic synergies after SCI reflect underlying neuropathology, the author performed morphometric assessments to quantify the degree of sparing tissue 4 weeks after SCI. Group 1 had 48–57% tissue sparing, group 2 had 43–51% sparing, and group 3 had 41–43% sparing (Figure 2-5). A significant difference was observed between groups ($F(2,15) = 18.93$, $p < 0.001$; one-way ANOVA with Tukey's post-hoc), suggesting that changes in kinematic synergy after SCI depend on the degree of sparing tissue. Moreover, since the SCI was performed from the dorsal side, the main

damage was on the dorsal side, and some tissue on the ventral side escaped fibrosis.

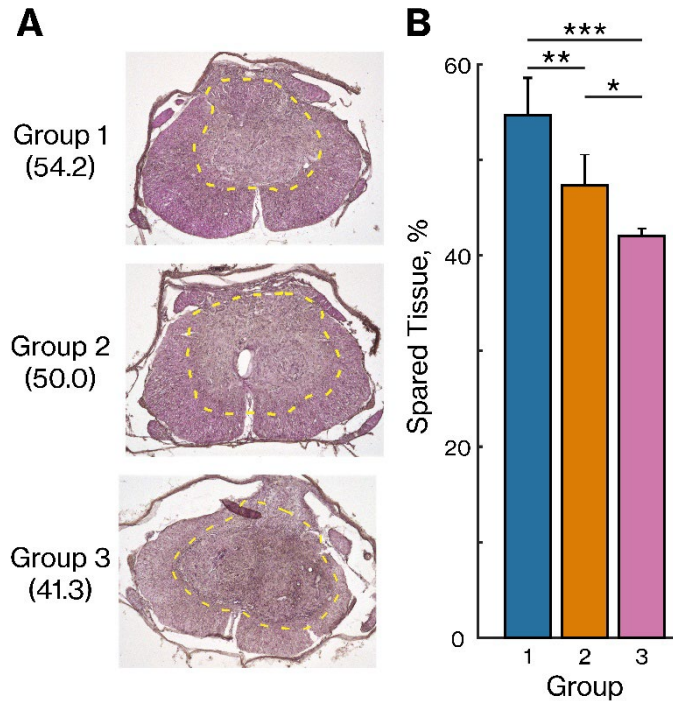


Figure 2-5. Spared tissue at the lesion epicenter

(A) Representative image of each of groups with lesion traces (surrounded by yellow line). The figure in parentheses indicates the degrees of spared tissue in each image.

(B) Mean (\pm SD) of degrees of spared tissue in each group (group 1, $n = 5$; group 2, $n = 7$; group 3, $n = 4$). Note that though the number of mice in group 1 was six, one spinal cord was not dissected due to technical issue. Comparisons were made with one-way ANOVA with Tukey's post-hoc multiple comparisons. Significance $* < 0.05$, $** < 0.01$, $*** < 0.001$.

2.4. Discussion

In the present study, the kinematic synergies were extracted by applying PCA to kinematic data of mice hindlimb during walking. Three synergy components were identified in intact mice, which represent forward propagation, forward/backward bent, and

upward/downward movement, respectively. The kinematic synergies in SCI mice were categorized into three groups using hierarchical cluster analysis based on the similarity of spatial components. The spatial components are different than those in intact mice in two groups. In the remaining group, the spatial components were similar to those of intact mice, but the temporal components were different. Moreover, a significant difference was observed between these three groups in histological damage of spinal cord. These results suggest the kinematic synergies of walking mice after SCI may be affected by the degree of damage.

The dimensionality reduction procedure using PCA identified first three synergies as spatial and temporal components, which described the essential features of walking in mice. The principal movements corresponding to PC₁ and PC₃ were forward propagation and upward/downward movement, respectively, which were consistent with previous findings in humans (Federolf et al., 2012; Stetter et al., 2020). The principal movements corresponding to PC₂ was visually identified as forward/backward bent because it was extracted in quadrupedal animals; however, it may be the component corresponding to the limb extension and limb flexion in human walking (Federolf et al., 2012; Ivanenko et al., 2007). Moreover, in the present study, the same spatial components were extracted when the mice changed the speed of their walking on a treadmill. This feature is consistent with the adaptability to environmental changes reported in humans (Lamoth et al., 2009) and monkeys (Courtine et al., 2005). These results confirm that the kinematic synergies extracted in mice have properties like the one extracted in previous studies in mice and many other different species (Catavittello et al., 2018).

The author identified three groups of kinematic synergies by applying hierarchical cluster analysis to spatial components extracted in SCI mice. In group 1, the

spatial components $W_{G1,1-3}$ did not change, while in group 2 and 3, mixing with different order components, such as $W_{\text{intact},2}$ $W_{\text{intact},3}$, was observed (Figure 2-3B,C). This mixture of different components observed in the present study is consistent with previous studies in SCI and stroke (Cheung et al., 2012; Ivanenko et al., 2013). These findings cause reduced independence of neural control signals of gait, which may affect the disability of adaptation to environmental change.

A significant difference was observed between these three groups in SCI mice in degree of spared tissue at the lesion epicenter by histological assessment. Although previous studies in SCI and stroke patients reported that distinct synergy patterns represent depending on the clinical severity (Barroso et al., 2015; Clark et al., 2010), it has not been investigated whether those patterns reflect structural damage of CNS. The modules, which are present in spinal cord, generate accurate walking pattern by integrating sensory input from limbs and motor command from brain (Poppele et al., 2002; Rossignol and Frigon, 2011). In this study, the spinal cord was injured from the dorsal side by IH impactor, and the spinal damage was mainly to dorsal column, where exists corticospinal tract (CST) and ascending pathways that transmit sensory information to the brain (Rossignol and Frigon, 2011). Therefore, the difference in the degree of damage between groups may reflect the difference in the degree of damage in the lateral and ventral funiculus, where exists the motor descending pathways, such as the rubrospinal and reticulospinal tracts (Rossignol and Frigon, 2011). In fact, group 2 and 3, severe groups, damaged descending tracts might affect the change in kinematic synergies.

In conclusion, the author showed that differences in kinematic synergies can be a pathophysiological indicator for SCI. Characterization of neuropathology of spinal cord might be crucial for the design and execution of clinical trials and for most appropriate

use of rehabilitation therapies (Freund et al., 2013), and these findings will be helpful for developing more effective rehabilitation and other treatment methods.

Chapter 3: Preserved Intersegmental Coordination of Locomotion in Spinal Cord Injury Common Marmosets

*This chapter was based on the following author's original article:

“Sato, Y., Kondo, T., Uchida, A., Sato, K., Yoshino-Saito, K., Nakamura, M., Okano, H., Ushiba, J., Preserved intersegmental coordination during locomotion after cervical spinal cord injury in common marmosets. *Behavioural Brain Research* 425, 113816 (9 pages).”

3.1. Introduction

In primates and humans, despite the regenerative failure of severed axons after SCI, partial lesions of the spinal cord are accompanied by some recovery of locomotor function (Curt et al., 2008; Friedli et al., 2015; Squair et al., 2021). However, they rarely achieve a similar level of gait function as unaffected people (Brotherton et al., 2007). Thus, patients with SCI may have locomotor control systems that are different from those of healthy individuals (Rossignol and Frigon, 2011), but these are not yet well understood.

There is a growing consensus that locomotor recovery depends on plasticity induced by the SCI (Friedli et al., 2015; Raineteau and Schwab, 2001; Willenberg and Steward, 2015). Plasticity of the descending pathways may involve regeneration of the damaged pathways and sprouting of undamaged pathways. This results in formation of new intrinsic spinal circuitry through new anatomical connections (new circuits) and strengthening of synaptic connectivity (enhancement of existing circuits) (Rossignol and Frigon, 2011). Examining how the locomotor output patterns change may be helpful in considering improved rehabilitation strategies (Ivanenko et al., 2013). Previous studies showed the locomotor patterns in SCI patients at thoracic spinal cord with body-weight

support treadmill have been found to be different from those of healthy individuals (Grasso et al., 2004), suggesting that the output locomotor patterns from the intrinsic spinal circuitry change over time due to neuroplasticity after SCI. However, it is not clear when and how the locomotor patterns change.

Kinematics analysis of the locomotor patterns can measure changes in the trajectory and joint angle (Battistuzzo et al., 2016; Shah et al., 2012). Additionally, it is important to validate intersegmental coordination. Intersegmental coordination is associated with the elevation angle of thigh, shank, and foot (Courtine et al., 2005; Grasso et al., 2004; Puentes et al., 2018a). When plotted against each other, human thigh, shank, and foot elevation angles covary to form a regular loop (i.e., gait loop) over a plane (Borghese et al., 1996). This planar law is thought to be responsible for the maintenance of dynamic equilibrium and adjustment of movement in response to environmental changes (Maclellan and McFadyen, 2010). This planar law is observed not only in humans but also in other mammals (Catavittello et al., 2018), such as dog (Catavittello et al., 2015), cats (Bosco et al., 2003) and monkeys (Courtine et al., 2005). The planar covariation is considered to be a common characteristic of intersegmental coordination controlled by CNS. Patients with stroke (Bleyenheuft et al., 2009; Chow and Stokic, 2015; Puentes et al., 2018b) or spinal disease (Grasso et al., 2004; Puentes et al., 2018a) often lack the planar covariation, but this showed improvements after rehabilitation. Furthermore, whether the planar covariation improves or not seems to be affected by the severity (Grasso et al., 2004). However, it is unclear how this planarity is impaired by lesion and how it recovers. Therefore, it is important to investigate the temporal changes in planarity.

In this study, the author analyzed the output of the locomotor pattern in a small

non-human primate, the common marmoset. The marmoset has received considerable attention in the fields of neuroscience and motor control because of its human-like CNS (Matsuzaki and Ebina, 2020; Okano, 2021; Prins et al., 2017). By following the walking ability from before injury to 12 weeks after unilateral hemisection at left cervical cord, the author investigates the temporal changes in basic kinematic parameters and intersegmental coordination over time.

3.2. Material and Methods

3.2.1. Animals

The current study used adult common marmosets (*Callithrix jacchus*; body weight, 300–400 g; n = 4). The animals were housed under a 12-h light/dark photoperiod, with food and water available ad libitum. All the animal experiments were approved by the Animal Research Committee of Keio University (approval number: 11006) and were conducted according to the guidelines of the National Institutes of Health.

3.2.2. Experimental procedures

Marmosets were anesthetized using an intramuscular injection of ketamine (30 mg/kg), xylazine (2.5 mg/kg), and atropine sulfate (0.05 mg/kg). Anesthesia was maintained by administering 1–1.5% isoflurane. Body temperature and oxygen saturation levels were monitored. After a laminectomy at the C3 or C4 level, the dura mater was incised longitudinally, and the left side of the spinal cord was cut at the C3/C4 or C4/C5 segment using a surgical blade. Efforts were made to minimize animal suffering. For 1 week after the operation, ampicillin (100 mg/kg) and butorphanol (0.015 mg/kg) was administered intramuscularly.

3.2.3. Open field scoring

To assess the locomotor recovery after SCI, open field test was performed from the time of the initial injury to 12 weeks after the operation. The open field test was developed for use in marmosets (Kitamura et al., 2011). The Lower Limb section of the open field rating scale was used to assess the motor function of the hindlimb (Table 3-1). Each marmoset was individually tested for 5 min on the floor and then in the cage to obtain the overall score (maximum 7 points).

Table 3-1. Lower Limb section of the open field rating scale

Range of motion & weight bearing	Slight movement of lower limbs	+ 0
	Extensive movement of lower limbs	+ 1
	Move forward with weight bearing of lower limbs	+ 1
	Jump	+ 1
	Jump successively	+ 1
Somatosensory	Drop lower limbs through gaps in the cage bars up to	
	Thigh	+ 0
	Knee	+ 1
	Foot only	+ 1
	Never drop	+ 1

3.2.4. Kinematic recording

Before recording the locomotion, the marmosets were habituated to the custom-made runway apparatus (length: 1,350 mm; width: 90 mm) constructed from a transparent acrylic board (thickness: 3 mm). A high-speed camera (150 frames/s, GX-3, nac Image Technology Inc., Tokyo, Japan), positioned on the left side (Figure 3-1), was used to record the marmosets walking at a self-selected speed for a total of 3–6 steps (Table 3-2)

in each of the following sessions: pre-operation (Pre), post-operation at 2 weeks (PO2w), PO6w, and PO12w.

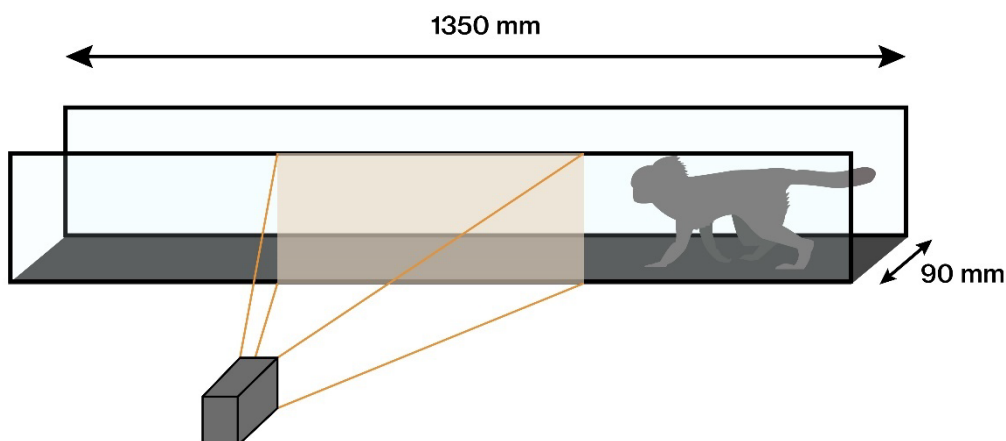


Figure 3-1. Schematic of runway for kinematic recording

Marmosets walked in the runway apparatus (length: 1,350 mm; width: 90 mm). The center of the runway, indicated by the orange area, were recorded by using a high-speed camera from left side.

Table 3-2. Number of trials

	Pre	PO2w	PO6w	PO12w
Marmoset A	6	3	5	5
Marmoset B	6	3	3	3
Marmoset C	4	3	3	4
Marmoset D	5	5	4	6

As in Chapter 2, no lateral impaired movement was observed after the injury, so the walking was recorded in the sagittal plane. Note here that this procedure has been commonly applied in previous papers on gait analysis (Friedli et al., 2015; Shimada et al., 2017; Wei et al., 2018). Reflective markers were attached (using an adhesive) to shaved

skin areas at MTP, ankle, knee, and hip (Figure 3-2).

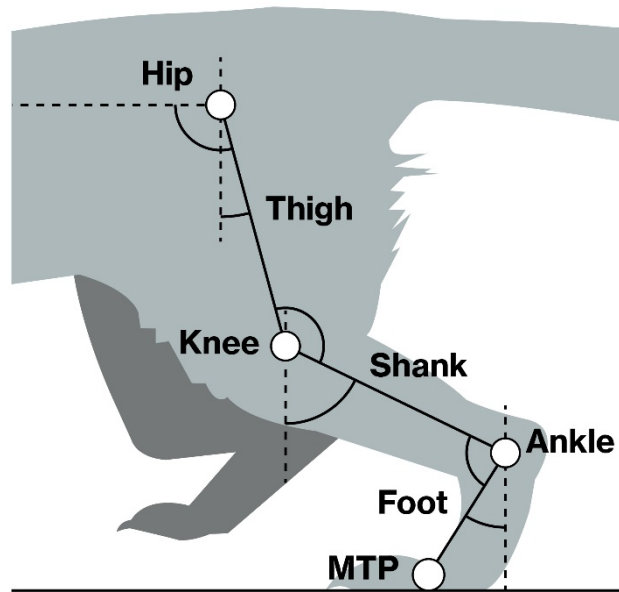


Figure 3-2. Locations of the tracked joints

Refractive markers were attached to four joints of each marmoset, namely MTP, ankle, knee, and hip.

The angle of each segment to the direction of gravity was computed as the elevation angle.

Each marker was tracked using Deeplabcut, a markerless pose estimation system based on transfer learning with deep neural network (Mathis et al., 2018). The standard DeepLabCut workflow was followed. Twenty training frames were randomly sampled from each session of each marmoset, and all parts of the training frames were manually labeled and used to train the network. Training was repeated for 200,000 iterations to reach a plateau in individual loss. The tracking accuracy validated with the frames that were not used for training was 3.5 pixels (~ 2 mm). Considering that the diameter of the reflective marker is 4 mm, the accuracy is sufficient to not significantly affect the kinematic data.

MATLAB 2020a (MathWorks, Inc., Natick, MA, USA) was used for data processing. Missing values of coordinates were filled using linear interpolation. Each cycle was defined as one paw contact to the next paw contact which were determined as the time when the MTP marker was at ground level, and subdivided into a stance phase and a swing phase based on the forward movement of the foot.

3.2.5. Endpoint trajectory

Endpoint trajectory was defined as the MTP joint position. To quantify the changes in endpoint trajectory, the author examined where the peak of the y-axis appeared during the swing phase. For this purpose, a/b was calculated, where b was the step length, calculated as the linear distance in the x-axis between the MTP positions from the beginning to the end of the swing phase. Moreover, a was calculated as the linear distance in the x-axis between the MTP positions from the beginning of the swing phase to when the peak of the y-axis.

3.2.6. Joint angle

The hindlimb was modeled as an interconnected chain of rigid segments to calculate the joint angles. The joint angle velocity was calculated as a derivative of the joint angle. In order to comprehensively evaluate the changes in joint angle, the maximum and minimum values of joint angles and angular velocities calculated from each trial in each session of each marmoset were pooled into one matrix, and PCA was applied. Scores obtained by projecting the data onto each eigenvector were compared between the sessions for each PC.

3.2.7. Planar covariation of elevation angle

To evaluate planar covariation representing intersegmental coordination, elevation angles were measured as the angles of segments to the direction of gravity (positive in forward direction) (Figure 3-2). Elevation angles have a much more stereotyped pattern than joint angles across individuals and trials (Bianchi et al., 1998; Borghese et al., 1996; Dewolf et al., 2018). Additionally, changes in the thigh, shank, and foot elevation angles covary linearly throughout the gait cycle. Plotting elevation angles in a three-dimensional space generates a gait loop for each cycle. PCA was applied to the concatenated matrices, including all cycle data from each session of each marmoset, to identify the best-fitting plane to the gait loops. The first two eigenvectors obtained from the PCA described the best-fitting plane. The planarity of the gait loop was quantified by the percentage of variance (PV), which accounted for of the third eigenvector. Higher planarity of the gait loop was associated with smaller variance; therefore, the variance was zero if the gait loop had perfect planarity. Moreover, the third eigenvector, corresponding to the normal of the plane, represented the plane orientation.

3.2.8. Correlation between hip-ankle distance and plane orientation

To examine the effect of changes in plane orientation, the author calculated their correlations with hip-ankle distance. Orientation of each plane was quantified by multiplying the variance by the thigh and shank coefficients ratio in PC2. The hip-ankle distance was defined as the linear distance between the two joints, normalized by the total length of thigh and shank of each marmoset.

3.2.9. Histology

For histological confirmation of the extent of the hemisection, all marmosets were anesthetized with pentobarbital sodium (100 mg/kg) and perfused with PBS (200 mL) and 4% paraformaldehyde (200 mL). Spinal cords were removed, postfixed in 4% PFA for 24 h, and exposed to 10%, 20%, and 30% sucrose for 24 h each. Transverse sections (50 μ m) were serially cut through the lesion area on a sliding microtome (REM-710; Yamato Kohki Industrial Co., Ltd, Saitama, Japan) and stained using 1% cresyl violet. A fluorescence microscope (BZ-8000, Keyence, Osaka, Japan) with objective lenses (CFI Plan Apo, 10 \times ; 0.45 numerical aperture; Nikon, Tokyo, Japan) was used to observe the sections, and the section with the largest sized lesion was designated the epicenter.

3.3. Results

3.3.1. Functional recovery after SCI

Figure 3-3A shows illustrations of the epicenter of hemisected marmosets. In all marmosets, the left side of the spinal cord was almost completely disrupted. The author assessed the pre- and post-operative motor function using an open field rating scale (Figure 3-3B). All marmosets achieved the maximum score of 7 before the operation. Although marmosets showed a functional loss in both the left forelimb and hindlimb immediately following the lesion surgery, they could move and turn over by using the non-paretic side and scored 2 points. The marmosets gradually recovered, reaching a plateau around 8–10 weeks after the operation. As in humans and other SCI models, a rapid decline in motor function was observed after SCI, followed by some degree of spontaneous recovery.

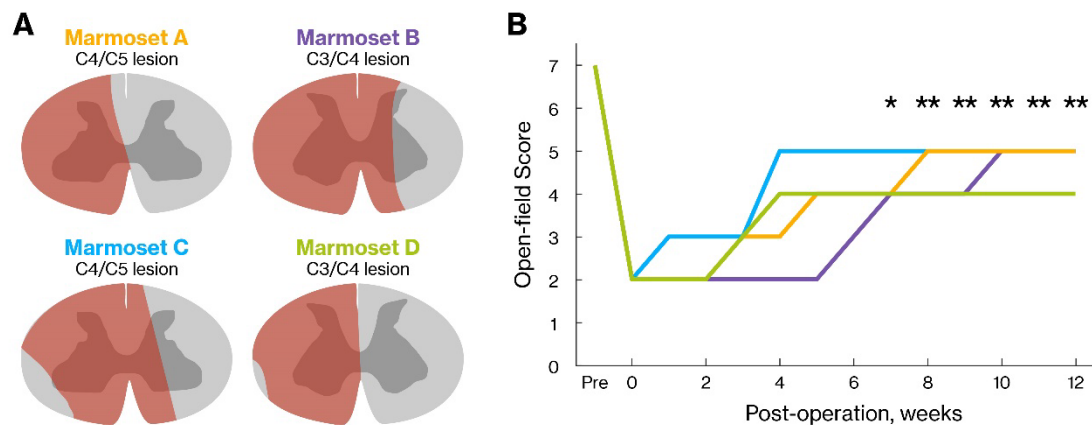


Figure 3-3. Lesion extent and open field scoring.

(A) Lesions produced by hemisection in the marmosets. Red indicates the damaged area. The lesions in marmosets A and C were located at the C4/C5 junction. The lesion in marmoset A extended into the left side of the spinal cord, sparing a small region of the dorsal funiculus. The lesion in marmoset C extended into the left side and slightly into the right side of the spinal cord, sparing a small region of the lateral funiculus. Lesions in marmosets B and D were located at the C3/C4 junction. The lesion in marmoset B extended into the left side and partially into the right side of the spinal cord. The lesion in marmoset D extended into the left side of the spinal cord, sparing a small region of the lateral funiculus.

(B) Mean (\pm SD) of the time course of motor function in hindlimb, representing an overview of the functional recovery of each marmoset recorded using the open field scale ($n = 4$). A gradual recovery of motor function was observed in each marmoset. * $p < 0.05$ and ** $p < 0.005$ for difference from 0 week after the operation; paired t -test.

3.3.2. Endpoint trajectory

The author recorded the marmoset gait on the runway at Pre, PO2w, PO6w, and PO12w, and applied signal processing in x- and y-coordinates of each joint. The marmosets did

not make a crouching or wide stance during the recording. Based on the previous studies (Courtine et al., 2005; Maier et al., 2009), basic gait parameters such as cycle duration, step length, duty factor, and gait speed were calculated (Figure 3-4A). Compared to the parameters of each session with Pre, duty factor of the left forelimb was significantly shorter at all time points, but other than that, a significant difference was observed only in cycle duration of PO12w. Although no significant difference was observed in other parameters, there was a trend such as a decrease in duty factor in PO2w and a gradual decrease in Gait speed. Figure 3-4B shows representative footfall patterns, which were determined visually from the videos in each session. In Pre, the footfall pattern was accomplished by paw contact with the diagonal legs showing the approximately same phase. As the author previously reported (Shimada et al., 2017), the gait in marmoset was like a trot gait. After the injury, the weight-bearing by the left forelimb was difficult, and the stance phase of the limb was short (Figure 3-1A). This capability recovered over time; however, the diagonal left hindlimb and right forelimb remained out-of-phase. The author plotted the left-right hindlimb coordination computed from footfall patterns in polar graphs (Figure 3-4C). In Pre, samples were clustered around 180° , corresponding to alternately and out-of-phase coordination. After the injury, the variation in samples increased, representing that the left-right coordination was poor.

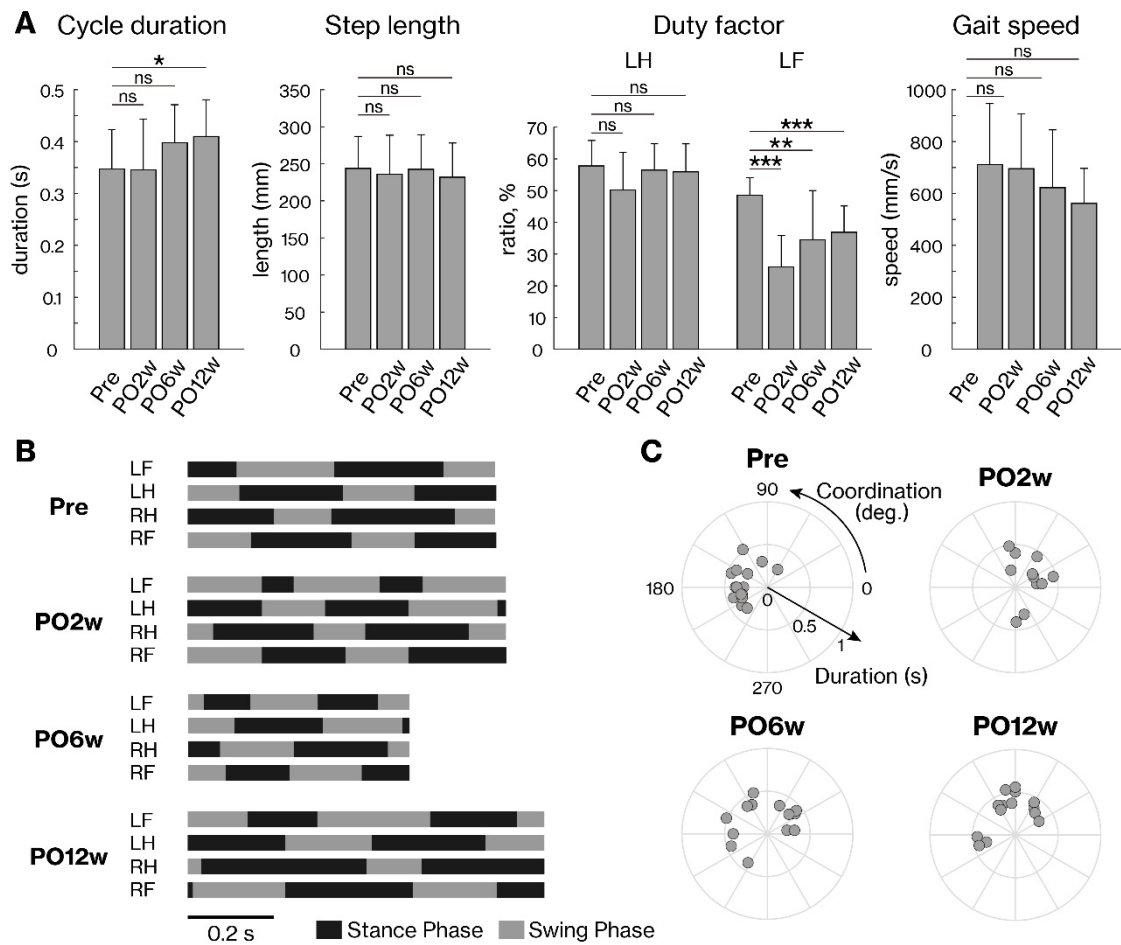


Figure 3-4. Changes in basic gait parameters and footfalls

(A) Mean (\pm SD) of basic gait parameters such as cycle duration, step length, duty factor (Left Hindlimb and Left Forelimb), and gait speed. Each value was calculated from all cycles of four marmosets. * $p < 0.05$; ns, no significant difference from Pre; one-way ANOVA followed by Dunnett's test as post hoc.

(B) Representative footfall patterns in four limbs. Black and gray boxes represent the duration of stance and swing phases of gait, respectively. LF, left forelimb; LH, left hindlimb; RH, right hindlimb; RF, right forelimb.

(C) Values of coordination between left and right hindlimbs in polar plots. Each dot corresponds to one cycle. The radius represents the cycle duration. The angular value represents the gap between the paw contact of the left and right hindlimbs during the cycle. If the limbs coordinate alternately and out

of phase, the angular value is 180°.

Next, to give insights into the control of foot motion, locomotion was represented by stick diagrams of the left hindlimb in one step cycle and by constructing endpoint trajectories for all the steps in each session (Figure 3-5A, B). These data showed that the coordinate changes after the operation were different from those at Pre. For instance, the timing of the peak of the y-axis at the endpoint had changed. Therefore, the author quantified a/b as shown in Figure 3-5C and found a significant increase in each post-operation session from Pre (Pre, 0.29 ± 0.05 ; PO2w, 0.51 ± 0.08 ; PO6w, 0.55 ± 0.08 ; PO12w, 0.52 ± 0.16 ; $p < 0.001$; one-way ANOVA followed by Dunnett's test as post hoc). The results showed that foot lift peaked early in the swing phase in Pre, whereas it shifted to a later stage after the operation, and no recovery was observed over time.

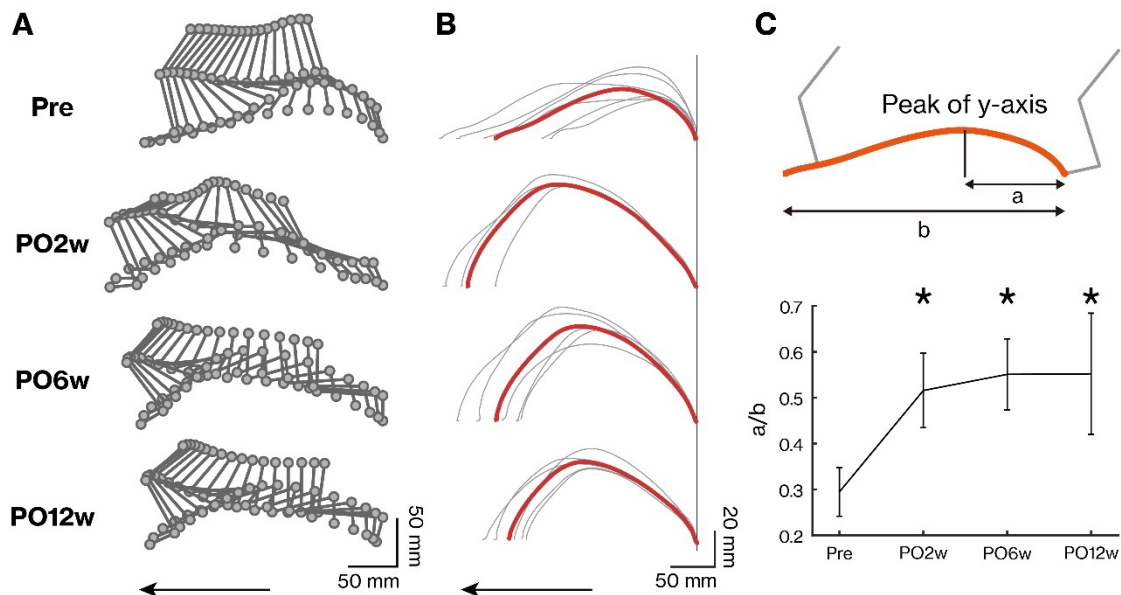


Figure 3-5. Changes in endpoint trajectory during each session

(A, B) Stick diagrams (A) and endpoint trajectories (B) of the hindlimb during swing phases. From

top to bottom, data from Pre, PO2w, PO6w, and PO12w are shown. The gray line in B indicates the trajectory aligned at the beginning of the swing phase of each step, and the red line indicates the mean trajectory.

(C) Schematic diagram of the definitions of a and b (upper panel) and mean (\pm SD) of all steps (Pre, $n = 21$; PO2w, $n = 12$; PO6w, $n = 16$; PO12w, $n = 18$) of a/b changes in four marmosets (lower panel). The results showed that a/b was larger post-operatively than pre-operatively, indicating that the peak of the y-axis was observed in the later stage of the swing phase. * $p < 0.001$ difference from Pre; one-way ANOVA followed by Dunnett's test as post hoc.

3.3.3. Joint angle

Figure 3-6A, B show the changes of joint angles and angle velocities in each session of a representative marmoset. To examine the changes in gait caused by SCI in terms of joint angles, PCA was applied to the maximum and minimum values of joint angle and angle velocity at each step, similar to the previous reports (DiGiovanna et al., 2016; Sato et al., in Press-b; Takeoka et al., 2014). The author visualized each step in the new space created by PC1–3 (Figure 3-6C). These three PCs explained almost 75% of the total variance in the data. There was large variance in the score projected to PC1 at PO2w and PO6w because of high variability of gait, while at PO12w, the scores were relatively clustered in the same position. However, a significant difference was observed between Pre and PO12w ($p < 0.05$; Welch's t-test with Bonferroni correction). PC2, with the second highest variance, distinguished between Pre and post-operative sessions ($p < 0.001$); whereas, PC3 did not distinguish between any of the sessions (Figure 3-6D). These data suggest that in addition to the endpoint trajectory, characteristics of the joint angle movement at PO12w were also altered from Pre. Moreover, the author calculated the

factor loadings, which correspond to correlations between the variable and PC1-3 (Figure 3-6E). In PC1, the absolute value of the loading factor was large for most of the parameters. However, the absolute value was large for the knee angle and the ankle minimum velocity in PC2.

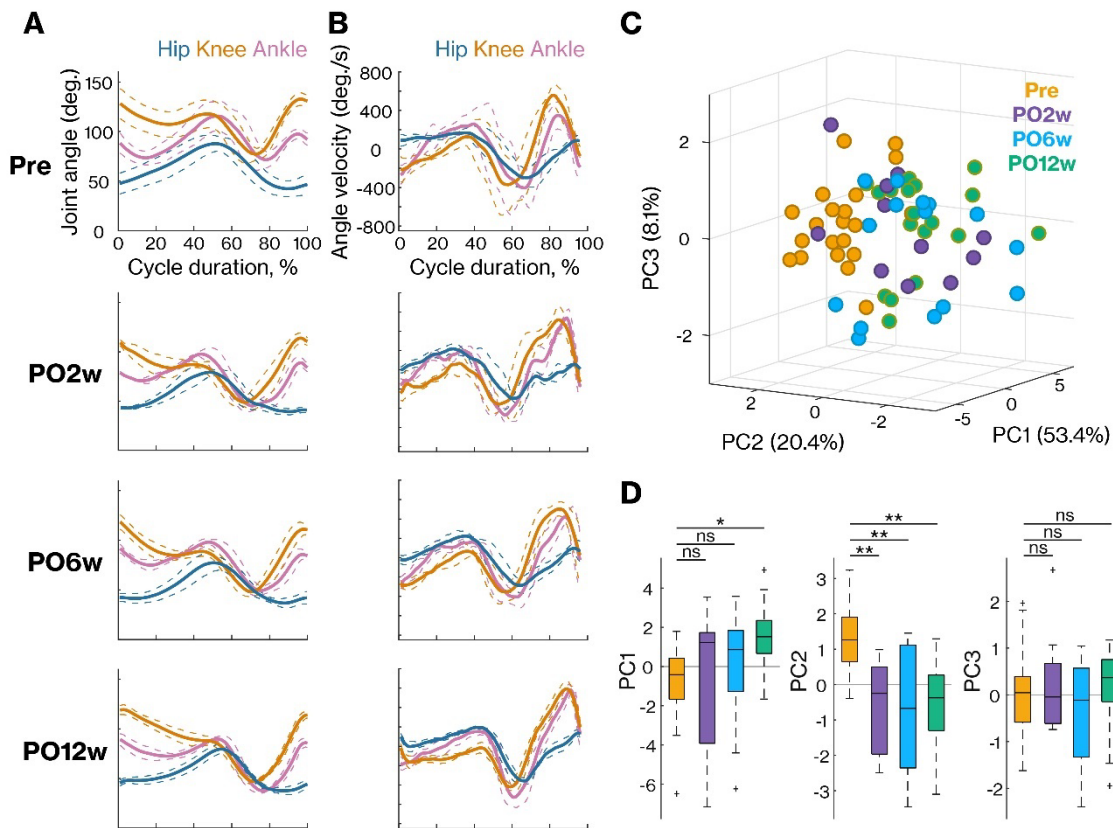


Figure 3-6. Principal component analysis applied to 12 computed joint angle parameters

(A) The mean waveforms (dotted lines, \pm SD) of joint angle of hip (blue), knee (orange), and ankle (purple) in each session. The maximum and minimum values in each trial were calculated to apply PCA.

(B) The mean waveforms (dotted lines, \pm SD) of angle velocity. The maximum and minimum values were calculated as well as the joint angles.

(C) Three-dimensional representation of joint angle parameters. Each dot indicates an individual step.

(D) Boxplots of the first three PCs. The scores of PC1, which showed the highest variance (43.5%), were significantly different between Pre and PO12w. PC2 distinguished between Pre and each post-operative session. * $p < 0.05$; ** $p < 0.001$; ns, no significant difference from Pre; Welch's t-test with Bonferroni correction.

(E) Loading factors on PC1–3. Brown and gray indicate positive and negative factors, respectively. H, hip; K, knee; A, ankle.

3.3.4. Planar covariation of the segment elevation angles

Figure 3-7A shows the mean (\pm SD) of the time-normalized elevation angle of three segments (thigh, shank, and foot) in each session of a representative marmoset. The intersegmental relationships and shapes of the waves showed changes. For instance, after the operation, the waveforms for the thigh and the foot were closer, and the slow change of shank observed for almost 40% of the cycle duration in Pre (see arrowhead in Figure 3-7A) had disappeared. Therefore, to examine the intersegmental coordination, these elevation angles of the thigh, shank, and foot were plotted against each other in 3-D space (Figure 3-7B). Overlaid each gray line in the figure represents the elevation angle change during each single cycle. This each line forms a loop because the marmosets generate cyclic gaits, i.e., the postures before and after each cycle are the same. Although time was not explicitly represented in these plots, time moves anticlockwise along the successive points (see arrows in Figure 3-7B). The beginning of the stance and the swing phase corresponds to the top and the bottom of the loop, respectively. The plane overlying each plot was determined by PCA to minimize the squared error. The eigenvectors of PC1 and PC2 correspond to the major and minor axes of the gait loop, respectively. The gait loops

were close to the plane, and PV of the eigenvector of PC3 (PV3) quantified the planarity. For the ideal plane, PV3 was 0. PV3 at Pre were $1.6 \pm 0.8\%$, $3.2 \pm 0.8\%$, $2.2 \pm 0.8\%$, and $1.1 \pm 0.7\%$ (mean \pm SD) for each marmoset, similar to the data previously reported for other quadrupedal mammals (Catavittello et al., 2015; Courtine et al., 2005). In addition, they reported that the plane orientation was parallel to the thigh axis in human (Ivanenko et al., 2007) (Figure 1-2A), while in quadruped primates, the orientation is rotated 45° around foot axis (Courtine et al., 2005) (Figure 1-2B), and in terms of the orientation, planes in marmoset were reflected the same characteristics as primates. Surprisingly, PV3 did not increase after the operation, especially at PO2w ($0.8\text{--}1.2\%$), suggesting that the intersegmental coordination was preserved during locomotion even in marmosets with SCI.

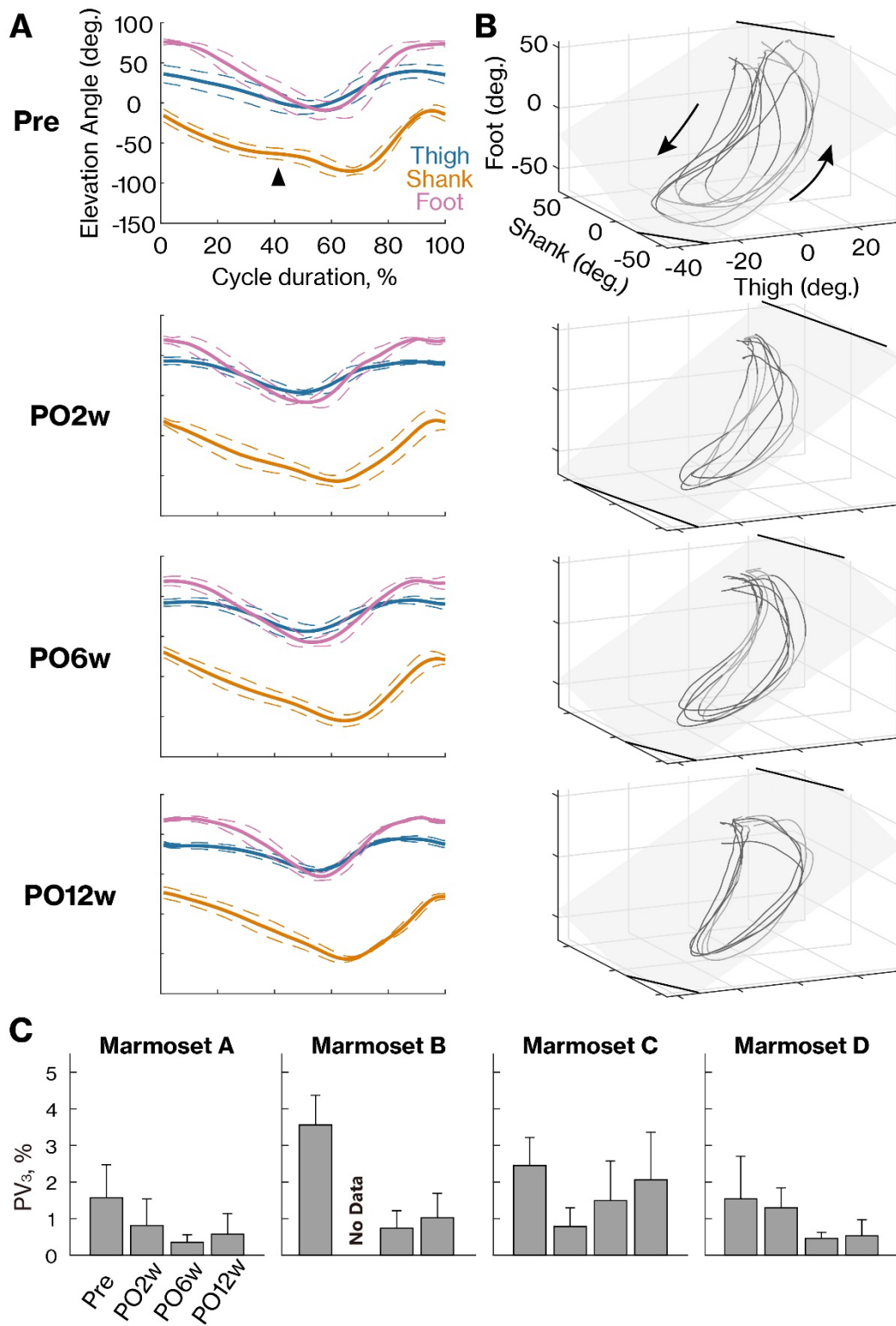


Figure 3-7. Planar covariation of the elevation angles

(A) The mean waveforms (dotted lines, \pm SD) of elevation angle of thigh (blue), shank (orange), and

foot (purple) in each session. The post-operative waveforms were different from those at Pre. The arrowhead indicates slow change of shank observed in only Pre.

(B) Gait loops of the normalized elevation angles at the thigh, shank, and foot in a representative marmoset. Plots for all trials performed in each session were superimposed on each other. Gait loops progress in time in the counterclockwise direction (the arrow in the top panel). The beginning of the stance and the swing phases corresponds to the top and bottom of the loops, respectively. The plane was determined by PCA to minimize the squared error.

(C) Mean (\pm SD) of the variance was accounted for by the PC3 (PV3). If PV3 was 0, the gait loop showed perfect planarity. PV3 remained low even after the operation. Since marmoset B did not have a stable gait at PO2w, no data are available.

The gait loops showed preserved planar covariation even after the operation, but there were different trends in the orientation of the planes (Figure 3-7B). In particular, the post-operative planes were rotated along the long axis of the gait loop with respect to the plane at Pre. To visualize the plane orientation in the three-dimensional space, the author plotted the plane normals for each session of a representative marmoset on the unit sphere (Figure 3-8A). The observed change in the plane normals was independent of the foot-axis, indicating that the change in the plane orientation was due to the relationship between the thigh and the shank. Therefore, the author plotted the plane normals for each marmoset when viewing the sphere from below (Figure 3-8B). The plane normals changed in a counterclockwise direction after the operation in all marmosets and appeared closer to Pre over time. These data suggest that thigh weighting increased and shank weighting decreased in the plane normals after the operation and that those weightings changed over time.

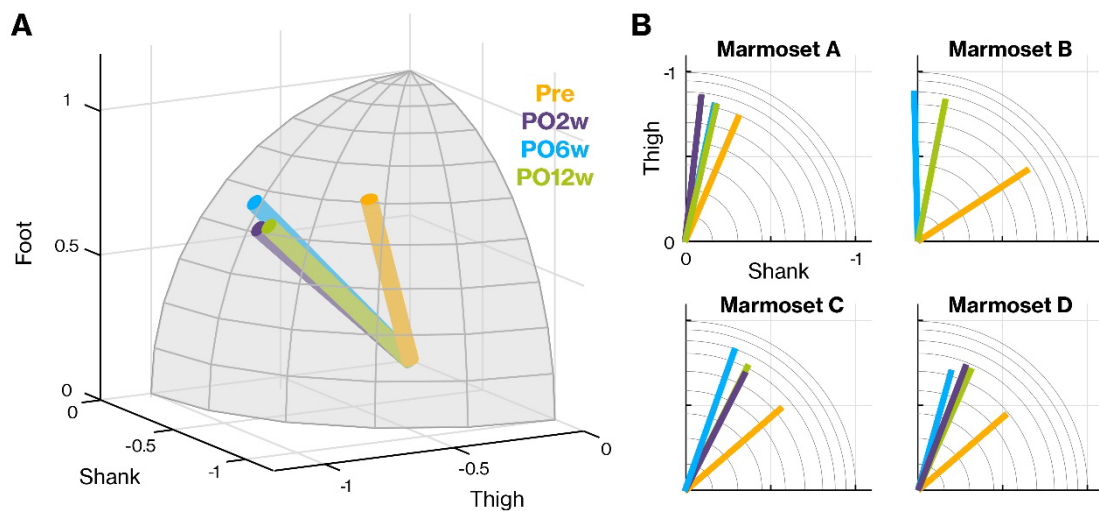


Figure 3-8. Orientation of the covariation plane for segment elevation angle

(A) The plane normal plotted on the unit sphere for each session of a representative marmoset. Each axis indicates the weighting of a segment in the plane normal. The weighting of the foot, corresponding to the latitude of the sphere surface, did not change in any session.

(B) Plane normal in each session laid on the thigh-shank plane. The lengths corresponded to the weighting of the foot. A change in the counterclockwise direction after the operation was observed in all marmosets. Note that the plane normals of PO2w and PO6w in marmoset C were similar. Since marmoset B did not have a stable gait at PO2w, no data are available.

Since thigh and shank connect the hip and ankle joints, a change in the weighting of these segments may affect the positional relationship between these joints. Therefore, the author measured the distance between the hip and ankle. Figure 3-9A shows the averaged time series of the distance in each session in a representative marmoset. The distance amplitude was larger post-operatively than at Pre. Thus, the author quantified the average amplitude and calculated its correlation with the ratio of the thigh to shank in PC2. A significant positive correlation was observed ($r = 0.53$, $p < 0.05$; Student's t-test)

(Figure 3-9B), suggesting that the change in the plane orientation reflected a change in the positional relationship of hip-ankle distance, which is consistent with previous studies (Dewolf et al., 2018; Ivanenko et al., 2007; Poppele et al., 2002).

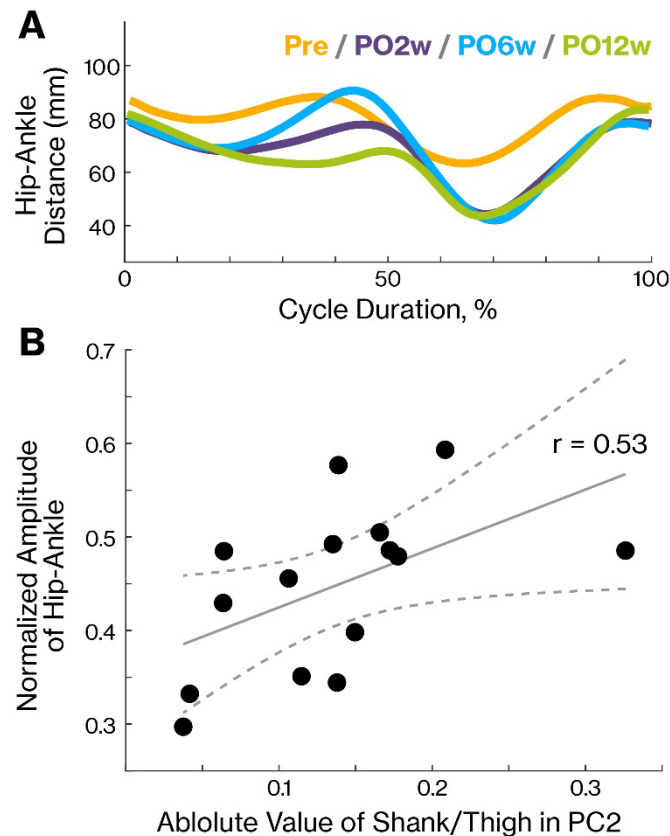


Figure 3-9. Positional relationship of hip and ankle joints

(A) Time series of the distance between the hip and ankle in each session of a representative marmoset. The waveforms were calculated as the average of all cycles in a session. The amplitude of the distance changed after the operation.

(B) Correlation between the amplitude of hip-ankle distance and ratio of thigh and shank weightings in PC2. The amplitude was calculated for each cycle, normalized by the length of the hindlimb, and averaged for all values of the session. A positive correlation was observed between the amplitude and the absolute value of the ratio ($p < 0.05$; Student's *t*-test). The dotted lines define 95% confidence

intervals.

3.4. Discussion

In this study, the author used the marmoset SCI model to analyze the kinematics data to examine the changes in the output locomotor pattern from the intraspinal circuits. Marmosets showed loss of detectable function in the left fore- and hindlimb immediately after the injury, but gradually recovered the ability to walk between 2 and 12 weeks post-operatively. The marmosets were able to walk relatively normally in an open field, but kinematics analysis showed changes in the endpoint trajectory and joint angle movement compared to those before the injury. The degree of recovery of these locomotor functions was consistent not only with previous reports in humans in the chronic phase but also with macaque monkey and rat hemiparetic models (Friedli et al., 2015). Additionally, planar covariation was preserved even 2 weeks after the SCI, suggesting that CNS maintains the coordination of the original elevation angle after unilateral hemisection at the cervical level in marmosets.

The results showed planar covariation was preserved at all time points from before the operation to 12 weeks after the injury. It has been confirmed that planar covariation of hindlimb may be controlled by CNS (Ivanenko et al., 2007; Ivanenko et al., 2008; Lacquaniti et al., 1999). Therefore, people with stroke or SCI, results in lack of the planar covariation. Additionally, the improvement in planarity correlated with recovery of the walking ability after rehabilitation (Grasso et al., 2004; Puentes et al., 2018a; Puentes et al., 2018b). However, the planarity in severely affected SCI patients did not improve (Grasso et al., 2004). Thus, recovery of locomotor function after CNS injury appears to correlate with the recovery of planarity. These relationships may partly

be explained by two reasons. The first is a spinal control mechanism in the quadrupedal marmoset. In this study, marmosets were able to walk with the fore- and hindlimbs of the injured side grounded two weeks after SCI (Figure 3-3B). On the other hand, despite unilateral brain damage, abnormal planar covariation is also found in the non-paretic side during waking in humans (Puentes et al., 2018b). Since the balance requirements in humans and marmosets are very different, the fact that the marmosets were walking while maintaining their balance after SCI is assumed to be the reason for the planarity preservation. Another factor in the maintenance of planar covariance is that it may reflect the connectivity of the supraspinal input and the spinal circuit. In the unilateral hemisection model, many spared pathways reached the spinal circuitry after hemisection; that is, these connections were maintained in the present study, resulting in preserving the planar covariation. It is important to note that planar covariation is not a trivial consequence of geometric and kinematic relationships (Catavittello et al., 2018; Ivanenko et al., 2008), and that the planarity in developmental and pathological locomotion is different from the normal (Cheron et al., 2001; Dominici et al., 2011). In fact, it is conceivable that the two factors may be combined, but it may be difficult to verify these factors in isolation.

While planar covariation remained constant over time, the orientation of the covariation plane differed due to different phase relationships between the thigh and shank (Figure 3-7). The covariation plane contains information about the body's inclination to gravity, which may be relevant to the adaptation to environmental changes (Barliya et al., 2009). The orientation of the plane depends on the animal species (Catavittello et al., 2018) and the inclined ground (Dewolf et al., 2018). In this study, the orientation was gradually changed after SCI, although marmosets walked on the runway

apparatus with no incline. This suggests a change in postural control within CNS of SCI marmosets. In fact, the distance between the marmoset's hip and ankle was less than that before the injury; therefore, the hindlimb position was similar to that while walking on an inclined ground. These orientations showed a left-right difference (data not shown), indicating asymmetry and lack of coordination of the left-right stepping phase, which may contribute to inefficient energy expenditure while walking.

The preservation of planar covariation found in this study may help to design new rehabilitation strategies. Until now, few facilities have introduced active gait rehabilitation for SCI patients in the early phase after injury, because the walking ability of people with SCI is severely impaired. Early, but not very early (Wahl et al., 2014), rehabilitation of these patients may be beneficial (Detloff et al., 2014) because rehabilitation promotes re-organization of the intraspinal circuits by engaging the remaining pathways and sensory afferents that supports locomotor recovery (Cote et al., 2017). This study suggested that intersegmental coordination function of the spinal circuit, which is one of the key factors required for adequate gait performance, is preserved even in the early stage after SCI. Although results from quadrupedal animals cannot be directly adapted to bipedal humans, the results of planarity preservation in primates, whose neural structure is similar to humans, may provide hope that active locomotor rehabilitation can be introduced during the early stage. Moreover, the content of the rehabilitation may be improved by using devices such as body-weight supported locomotor training (Cote et al., 2017) and robot-assisted gait training, such as Lokomat (Nam et al., 2017) and HAL® (Puentes et al., 2018a), which take planar covariation into consideration.

Chapter 4: Conclusion

The purpose of the research in this dissertation was to apply the evaluation system that focuses on coordination for disturbed locomotion after SCI to explore the changes in coordinated joint movement that underlies the gait generation. In Chapter 2, the author investigated the differences in locomotor output patterns in mice with varying degrees of injury to obtain proof of the analysis and found differences in kinematic coordination may reflect underlying SCI neuropathology. In order to verify whether the analysis method is adaptable to humans in the future, Chapter 3 describes the temporal change of kinematic coordination after SCI in marmosets and found that intersegmental coordination represented by planar covariation was preserved overtime after the injury.

Although the experiments in this dissertation provided important evidence for understanding the potential mechanisms involved in the recovery of locomotion, detailed neurological exploration may be further needed. In this study, the author has only assessed the degree of spared tissue at the lesion epicenter of the spinal cord to investigate the CNS status. However, as mentioned in Chapters 2, the spinal modular structure dynamically interacts with inputs from several descending pathways such as CST, reticulospinal tract (RST), and propriospinal tract for adapting and modulating locomotion (Rossignol and Frigon, 2011). Each tract originates from a different region and contributes differently to locomotor control. For example, RST originates from the reticular formation of the brainstem and is mainly involved in gross movements and postural control, resulting in severe gait disturbance after this pathway is damaged. Furthermore, it shows little plasticity in spontaneous recovery. On the other hand, CST originates from the cortex, is involved in fine movements, and has higher plasticity and potential to create new pathways than RST. In addition, this plasticity may be high, especially in primates. Hence,

pathway-specific reconnection after injuries will also result in differences in gait patterns. For example, it has been suggested that the degree of CST recovery correlates with recovery of gait function (Friedli et al., 2015). In addition, it was demonstrated that after CST lesions in rats, new connections could be established with the lumbosacral cord through cervical propriospinal tracts (Figure 4-1A) (Bareyre et al., 2004). Propriospinal tracts appear to be of considerable importance for volitional aspects of locomotor recovery in other species such as mice (Courtine et al., 2008) and cats (Kato et al., 1984), through the formation of new functional circuits (Figure 4-1B). RST reorganization does not occur spontaneously, but after treadmill training in SCI rats, reconnection beyond the lesion was observed and voluntary stepping ability was recovered (Figure 4-1C) (Asboth et al., 2018). However, it is unclear how the changes in these pathways relate to the modules in spinal cord, and it is important to investigate the extent to which axons in each pathway remain or regenerate functional after SCI. To approach these problems, it is desirable to use neural tracers to visualize each pathway and to verify the relationship between the degree of remained axons of each pathway and locomotor output pattern. Furthermore, there remains a large knowledge gap in identifying the specific roles played by these different pathways (Frigon, 2017). Genetic manipulation of specific neuronal populations (Takeoka et al., 2014) or selective excision of specific pathways using toxins or viral system (Luo et al., 2018) is a powerful approach to elucidate the neural organization of locomotor networks.

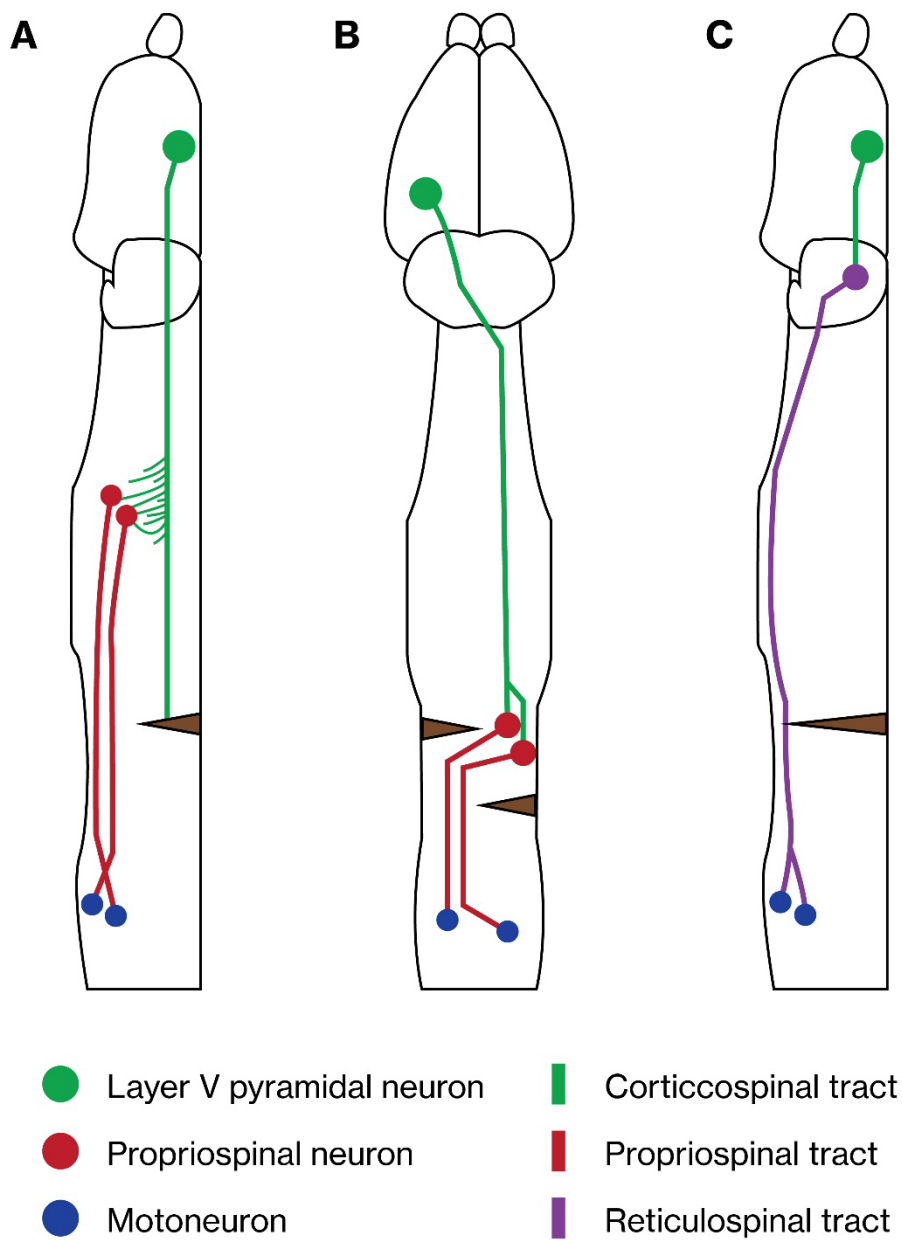


Figure 4-1. Schematic representation of new connection after SCI in rat

(A) Corticospinal-propriospinal detour circuit is generated after SCI.

(B) Propriospinal tract generates a new circuit after spatially separated complete lesion (staggered hemisection).

(C) Reticulospinal tract, which does not regenerate spontaneously, is rewired beyond the lesion area after treadmill training (modified from Loy and Bareyre (2019)).

Focusing on the locomotor output pattern generated by the spinal module, rather than the basic kinematic parameters such as step length, cycle duration, speed after SCI, suggests the possibility to real-world applications, such as locomotor rehabilitation of patients with SCI. However, the author should still be cautious about directly translate these findings obtained in animal models to humans. For example, humans are bipedal, while mice and marmosets are quadrupedal. This may lead to significant differences in neural control mechanisms such as basic postural control, center of gravity, and coordination of upper and lower limbs, as well as in compensatory strategies after SCI.

Furthermore, the balance requirements in bipedal human also differ from those in quadrupedal animals and require more careful interpretation. On the other hand, it has been suggested that there are common mechanisms that are common to humans. For example, the coordination between the arms and legs is often impaired, or even absent, in people with incomplete SCI, and leg muscle activity induced by passive locomotor-like movements was modulated by passive and active arm movements in subjects with an incomplete SCI at cervical levels (Kawashima et al., 2008), and others also reported that movement of the arms improved the pattern of leg muscle activation in subjects with incomplete SCI (Visintin and Barbeau, 1994). Also, a recent study showed that a kinematic synergy involving the planar covariation of limb holds in 54 different animal species (10 birds and 44 mammals), despite significant differences in body size and mass (from 30 g to 4 tons), limb configuration, and bipedal and quadrupedal gait (Catavittello et al., 2018).

The author can see that the accumulation of findings in animals is significant enough to be applied to humans; however, the author believes that clinical research in

humans is also needed in parallel with animal research to close the gap between animal and human research through these studies. In recent years, the resolution of MRI has improved, and it is possible to verify the relationship between locomotor output pattern and spinal damage estimated by MRI in humans over time. This relationship may be revealed in a clinical situation.

Overall, the author established and characterized interlimb coordination in locomotion after SCI to extract CNS features to understand post-SCI CNS function. The result provides a roadmap for how to analyze the impaired locomotion and the recovery process after SCI in order to understand CNS as a skillful controller. This is the important implication of this dissertation. Moreover, the locomotor coordination analysis can be applied as an objective functional evaluation of a patient's progress during a rehabilitation program. A recent study showed that when robot-assisted rehabilitation by HAL® was performed on patients with an idiopathic degenerative spinal disease, the coincident improvement of the clinical evaluation of functional score and the recovery of intersegmental coordination, suggesting an association between the changes in the walking performance and locomotor coordination pattern (Puentes et al., 2018a). Thus, this method has the potential for a biomarker of the state of spinal cord pathology after injury. The author concludes this dissertation with the hope that this research will contribute to the development of neuroscience and neurotherapy.

Acknowledgements

This dissertation has been written under the direction and guidance on Associate Professor Junichi Ushiba in Department of Biosciences and Informatics, Faculty of Science and Technology, Keio University, Japan.

I would like to thank all the people who have helped me during my Ph.D. experiments and writing of this dissertation. I particularly appreciate:

My supervisor:

Associate Professor **Junichi Ushiba** for his contentions support, inspiration, creativity, and enthusiasm since I was a bachelor student. Thanks to his unique and sophisticated philosophy in science, I could have finished my Ph.D. study. His guidance helped me in not only the time of research but also daily life. I would like to express my deepest appreciation to him.

My committee members:

Professor **Kotaro Oka**, Associate Professor **Kohji Hotta** in Department of Biosciences and Informatics, and Professor **Masaki Takahashi** in Department of System Design Engineering for agreeing to sit on my committee. Their valuable comments improved my Ph.D. study.

My advisor:

Assistant Professor **Takahiro Kondo** in Department of Physiology, Keio University School of Medicine for his enormous contribution to my Ph.D. study. Without his guidance and persistent help, this dissertation would not have materialized. Furthermore,

his continuous support, which started when I was an undergraduate, has also helped me grow as a person. I owe a very important debt to him.

All the current and past members of Ushiba laboratory, particularly the following:

Dr. **Akito Kosugi**, Mr. **Kenta Sato**, Mr. **Akito Uchida**, Mr. **Katsuya Sakuyama**, Mr. **Masaki Otaka**, Mr. **Takafumi Nakamura**, Ms. **Momoka Tanaka**, Ms. **Risa Saito**, and Mr. **Daijiro Hara** for their help with the animal experiments and for being fun.

Dr. **Shoko Kasuga** for her thoughtful guidance when I was an undergraduate and master's student.

Ms. **Sayoko Ishii**, Ms. **Kumi Nanjo**, Ms. **Shoko Tonomoto**, Ms. **Aya Kamiya**, and Ms. **Yumiko Kakubari** for their support on a daily basis. Thanks to them, I enjoyed my research comfortably every day.

My collaborators in Keio University School of Medicine, Japan:

Professor **Hideyuki Okano** for allowing me to do my Ph.D. study in his laboratory. I will never forget the many resources you gave me, such as experimental room and equipment and valuable discussions.

Dr. **Kimika Yoshino** for her help with the animal experiments.

Dr. **Reona Kobayashi** for her kindness. Without her kindhearted support, I would have faltered many times.

I want to thank all my friends, and special thanks go to the members of Bubb-lou Ushiba, Mr. **Wataru Tsuchihashi**, Dr. **Kosugi Akito**, Mr. **Kenta Sato**, Dr. **Shoichiro Takeda**, Mr. **Hirokazu Suzuki**, Mr. **Katsuya Sakuyama**, Mr. **Gaku Shiraishi**, Mr. **Shohei Kimura**,

Mr. **Daijiro Hara**, whose love and support have always been motivating me and making my life more enjoyable.

Lastly, and most importantly, I would like to express my heartfelt gratitude to my parents, **Manabu** and **Eko Sato**. They have always given me unconditional love. Without them, I would not be who I am today. Many thanks for supporting me in my decision to go on to a Ph.D. degree.

To them I dedicate this dissertation.

Funding

This work was supported by RIKEN Junior Research Associate Program.

References

- Alluin, O., Karimi-Abdolrezaee, S., Delivet-Mongrain, H., Leblond, H., Fehlings, M.G., Rossignol, S., 2011. Kinematic study of locomotor recovery after spinal cord clip compression injury in rats. *Journal of Neurotrauma* 28, 1963-1981.
- Aoi, S., Funato, T., 2016. Neuromusculoskeletal models based on the muscle synergy hypothesis for the investigation of adaptive motor control in locomotion via sensory-motor coordination. *Neuroscience Research* 104, 88-95.
- Aoi, S., Ohashi, T., Bamba, R., Fujiki, S., Tamura, D., Funato, T., Senda, K., Ivanenko, Y., Tsuchiya, K., 2019. Neuromusculoskeletal model that walks and runs across a speed range with a few motor control parameter changes based on the muscle synergy hypothesis. *Scientific Reports* 9, 369 (13 pages).
- Asboth, L., Friedli, L., Beauparant, J., Martinez-Gonzalez, C., Anil, S., Rey, E., Baud, L., Pidpruzhnykova, G., Anderson, M.A., Shkorbatova, P., Batti, L., Pagès, S., Kreider, J., Schneider, B.L., Barraud, Q., Courtine, G., 2018. Cortico-reticulo-spinal circuit reorganization enables functional recovery after severe spinal cord contusion. *Nature Neuroscience* 21, 576-588.
- Barbeau, H., Ladouceur, M., Norman, K.E., Pepin, A., Leroux, A., 1999. Walking after spinal cord injury: Evaluation, treatment, and functional recovery. *Archives of Physical Medicine and Rehabilitation* 80, 225-235.
- Bareyre, F.M., Kerschensteiner, M., Raineteau, O., Mettenleiter, T.C., Weinmann, O., Schwab, M.E., 2004. The injured spinal cord spontaneously forms a new intraspinal circuit in adult rats. *Nature Neuroscience* 7, 269-277.
- Barliya, A., Omlor, L., Giese, M.A., Flash, T., 2009. An analytical formulation of the law of intersegmental coordination during human locomotion. *Experimental Brain Research* 193, 371-385.
- Barroso, F.O., Torricelli, D., Bravo-Esteban, E., Taylor, J., Gomez-Soriano, J., Santos, C., Moreno, J.C., Pons, J.L., 2015. Muscle synergies in cycling after incomplete spinal cord injury: Correlation with clinical measures of motor function and spasticity. *Frontiers in Human Neuroscience* 9, 706 (16 pages).
- Battistuzzo, C.R., Rank, M.M., Flynn, J.R., Morgan, D.L., Callister, R., Callister, R.J., Galea, M.P., 2016. Gait recovery following spinal cord injury in mice: Limited effect of treadmill training. *Journal of Spinal Cord Medicine* 39, 335-343.
- Bianchi, L., Angelini, D., Orani, G.P., Lacquaniti, F., 1998. Kinematic coordination in human gait: Relation to mechanical energy cost. *Journal of Neurophysiology* 79, 2155-2170.
- Bizzi, E., Cheung, V.C., 2013. The neural origin of muscle synergies. *Frontiers in*

- Computational Neuroscience 7, 51 (6 pages).
- Bizzi, E., Mussa-Ivaldi, F.A., Giszter, S., 1991. Computations underlying the execution of movement: A biological perspective. *Science* 253, 287-291.
- Bleyenheuft, C., Cockx, S., Caty, G., Stoquart, G., Lejeune, T., Detrembleur, C., 2009. The effect of botulinum toxin injections on gait control in spastic stroke patients presenting with a stiff-knee gait. *Gait and Posture* 30, 168-172.
- Borghese, N.A., Bianchi, L., Lacquaniti, F., 1996. Kinematic determinants of human locomotion. *Journal of Physiology* 494, 863-879.
- Bosco, G., Rankin, A., Poppele, R.E., 2003. Modulation of dorsal spinocerebellar responses to limb movement. I. Effect of serotonin. *Journal of Neurophysiology* 90, 3361-3371.
- Brotherton, S.S., Krause, J.S., Nietert, P.J., 2007. Falls in individuals with incomplete spinal cord injury. *Spinal Cord* 45, 37-40.
- Calancie, B., Molano, M.R., Broton, J.G., 2002. Interlimb reflexes and synaptic plasticity become evident months after human spinal cord injury. *Brain* 125, 1150-1161.
- Calancie, B., Needham-Shropshire, B., Jacobs, P., Willer, K., Zych, G., Green, B.A., 1994. Involuntary stepping after chronic spinal cord injury. Evidence for a central rhythm generator for locomotion in man. *Brain* 117 1143-1159.
- Cappellini, G., Ivanenko, Y.P., Poppele, R.E., Lacquaniti, F., 2006. Motor patterns in human walking and running. *Journal of Neurophysiology* 95, 3426-3437.
- Catavittello, G., Ivanenko, Y., Lacquaniti, F., 2018. A kinematic synergy for terrestrial locomotion shared by mammals and birds. *Elife* 7 (28 pages).
- Catavittello, G., Ivanenko, Y.P., Lacquaniti, F., 2015. Planar covariation of hindlimb and forelimb elevation angles during terrestrial and aquatic locomotion of dogs. *PloS One* 10, e0133936 (26 pages).
- Cha, J., Heng, C., Reinkensmeyer, D.J., Roy, R.R., Edgerton, V.R., De Leon, R.D., 2007. Locomotor ability in spinal rats is dependent on the amount of activity imposed on the hindlimbs during treadmill training. *Journal of Neurotrauma* 24, 1000-1012.
- Cheron, G., Bouillot, E., Dan, B., Bengoetxea, A., Draye, J.P., Lacquaniti, F., 2001. Development of a kinematic coordination pattern in toddler locomotion: Planar covariation. *Experimental Brain Research* 137, 455-466.
- Cheung, V.C., Piron, L., Agostini, M., Silvoni, S., Turolla, A., Bizzi, E., 2009. Stability of muscle synergies for voluntary actions after cortical stroke in humans. *Proceedings of the National Academy of Sciences of the United States of America* 106, 19563-19568.
- Cheung, V.C., Turolla, A., Agostini, M., Silvoni, S., Bennis, C., Kasi, P., Paganoni, S.,

- Bonato, P., Bizzi, E., 2012. Muscle synergy patterns as physiological markers of motor cortical damage. *Proceedings of the National Academy of Sciences of the United States of America* 109, 14652-14656.
- Chow, J.W., Stokic, D.S., 2015. Intersegmental coordination of gait after hemorrhagic stroke. *Experimental Brain Research* 233, 125-135.
- Chvatal, S.A., Torres-Oviedo, G., Safavynia, S.A., Ting, L.H., 2011. Common muscle synergies for control of center of mass and force in nonstepping and stepping postural behaviors. *Journal of Neurophysiology* 106, 999-1015.
- Clark, D.J., Ting, L.H., Zajac, F.E., Neptune, R.R., Kautz, S.A., 2010. Merging of healthy motor modules predicts reduced locomotor performance and muscle coordination complexity post-stroke. *Journal of Neurophysiology* 103, 844-857.
- Cote, M.P., Murray, M., Lemay, M.A., 2017. Rehabilitation strategies after spinal cord injury: Inquiry into the mechanisms of success and failure. *Journal of Neurotrauma* 34, 1841-1857.
- Courtine, G., Roy, R.R., Hodgson, J., McKay, H., Raven, J., Zhong, H., Yang, H., Tuszynski, M.H., Edgerton, V.R., 2005. Kinematic and emg determinants in quadrupedal locomotion of a non-human primate (rhesus). *Journal of Neurophysiology* 93, 3127-3145.
- Courtine, G., Schieppati, M., 2004. Tuning of a basic coordination pattern constructs straight-ahead and curved walking in humans. *Journal of Neurophysiology* 91, 1524-1535.
- Courtine, G., Song, B., Roy, R.R., Zhong, H., Herrmann, J.E., Ao, Y., Qi, J., Edgerton, V.R., Sofroniew, M.V., 2008. Recovery of supraspinal control of stepping via indirect propriospinal relay connections after spinal cord injury. *Nature Medicine* 14, 69-74.
- Curt, A., Van Hedel, H.J., Klaus, D., Dietz, V., Group, E.-S.S., 2008. Recovery from a spinal cord injury: Significance of compensation, neural plasticity, and repair. *Journal of Neurotrauma* 25, 677-685.
- Daffertshofer, A., Lamoth, C.J., Meijer, O.G., Beek, P.J., 2004. Pca in studying coordination and variability: A tutorial. *Clinical Biomechanics (Bristol, Avon)* 19, 415-428.
- Davis, B.L., Vaughan, C.L., 1993. Phasic behavior of emg signals during gait: Use of multivariate statistics. *Journal of Electromyography and Kinesiology* 3, 51-60.
- De Quervain, I.A., Simon, S.R., Leurgans, S., Pease, W.S., McAllister, D., 1996. Gait pattern in the early recovery period after stroke. *Journal of Bone and Joint Surgery (American Volume)* 78, 1506-1514.

- Den Otter, A.R., Geurts, A.C., Mulder, T., Duysens, J., 2007. Abnormalities in the temporal patterning of lower extremity muscle activity in hemiparetic gait. *Gait and Posture* 25, 342-352.
- Detloff, M.R., Smith, E.J., Quiros Molina, D., Ganzer, P.D., Houle, J.D., 2014. Acute exercise prevents the development of neuropathic pain and the sprouting of non-peptidergic (gdnf- and artemin-responsive) c-fibers after spinal cord injury. *Experimental Neurology* 255, 38-48.
- Dewolf, A.H., Ivanenko, Y., Zelik, K.E., Lacquaniti, F., Willems, P.A., 2018. Kinematic patterns while walking on a slope at different speeds. *Journal of Applied Physiology* 125, 642-653.
- Dietz, V., Muller, R., Colombo, G., 2002. Locomotor activity in spinal man: Significance of afferent input from joint and load receptors. *Brain* 125, 2626-2634.
- DiGiovanna, J., Dominici, N., Friedli, L., Rigosa, J., Duis, S., Kreider, J., Beauparlant, J., van den Brand, R., Schieppati, M., Micera, S., Courtine, G., 2016. Engagement of the rat hindlimb motor cortex across natural locomotor behaviors. *Journal of Neuroscience* 36, 10440-10455.
- Dobkin, B.H., 2000. Functional rewiring of brain and spinal cord after injury: The three rs of neural repair and neurological rehabilitation. *Current Opinion in Neurology* 13, 655-659.
- Dominici, N., Ivanenko, Y.P., Cappellini, G., d'Avella, A., Mondì, V., Cicchese, M., Fabiano, A., Silei, T., Di Paolo, A., Giannini, C., Poppele, R.E., Lacquaniti, F., 2011. Locomotor primitives in newborn babies and their development. *Science* 334, 997-999.
- Federolf, P., Tecante, K., Nigg, B., 2012. A holistic approach to study the temporal variability in gait. *Journal of Biomechanics* 45, 1127-1132.
- Fiander, M.D., Stifani, N., Nichols, M., Akay, T., Robertson, G.S., 2017. Kinematic gait parameters are highly sensitive measures of motor deficits and spinal cord injury in mice subjected to experimental autoimmune encephalomyelitis. *Behavioural Brain Research* 317, 95-108.
- Fong, A.J., Cai, L.L., Otsoshi, C.K., Reinkensmeyer, D.J., Burdick, J.W., Roy, R.R., Edgerton, V.R., 2005. Spinal cord-transected mice learn to step in response to quipazine treatment and robotic training. *The Journal of Neuroscience* 25, 11738-11747.
- Franklin, S.B., Gibson, D.J., Robertson, P.A., Pohlmann, J.T., Fralish, J.S., 1995. Parallel analysis - a method for determining significant principal components. *Journal of Vegetation Science* 6, 99-106.

- Freund, P., Seif, M., Weiskopf, N., Friston, K., Fehlings, M.G., Thompson, A.J., Curt, A., 2019. Mri in traumatic spinal cord injury: From clinical assessment to neuroimaging biomarkers. *Lancet Neurology* 18, 1123-1135.
- Freund, P., Weiskopf, N., Ashburner, J., Wolf, K., Sutter, R., Altmann, D.R., Friston, K., Thompson, A., Curt, A., 2013. Mri investigation of the sensorimotor cortex and the corticospinal tract after acute spinal cord injury: A prospective longitudinal study. *Lancet Neurology* 12, 873-881.
- Friedli, L., Rosenzweig, E.S., Barraud, Q., Schubert, M., Dominici, N., Awai, L., Nielson, J.L., Musienko, P., Nout-Lomas, Y., Zhong, H., Zdunowski, S., Roy, R.R., Strand, S.C., van den Brand, R., Havton, L.A., Beattie, M.S., Bresnahan, J.C., Bezaud, E., Bloch, J., Edgerton, V.R., Ferguson, A.R., Curt, A., Tuszynski, M.H., Courtine, G., 2015. Pronounced species divergence in corticospinal tract reorganization and functional recovery after lateralized spinal cord injury favors primates. *Science Translational Medicine* 7, 302ra134 (12 pages).
- Frigon, A., 2017. The neural control of interlimb coordination during mammalian locomotion. *Journal of Neurophysiology* 117, 2224-2241.
- Funato, T., Aoi, S., Oshima, H., Tsuchiya, K., 2010. Variant and invariant patterns embedded in human locomotion through whole body kinematic coordination. *Experimental Brain Research* 205, 497-511.
- Gil-Agudo, A., Perez-Nombela, S., Forner-Cordero, A., Perez-Rizo, E., Crespo-Ruiz, B., del Ama-Espinosa, A., 2011. Gait kinematic analysis in patients with a mild form of central cord syndrome. *Journal of Neuroengineering and Rehabilitation* 8, 7 (10 pages).
- Gizzi, L., Nielsen, J.F., Felici, F., Ivanenko, Y.P., Farina, D., 2011. Impulses of activation but not motor modules are preserved in the locomotion of subacute stroke patients. *Journal of Neurophysiology* 106, 202-210.
- Goldberg, E.J., Neptune, R.R., 2007. Compensatory strategies during normal walking in response to muscle weakness and increased hip joint stiffness. *Gait and Posture* 25, 360-367.
- Gracia-Ibanez, V., Sancho-Bru, J.L., Vergara, M., Jarque-Bou, N.J., Roda-Sales, A., 2020. Sharing of hand kinematic synergies across subjects in daily living activities. *Scientific Reports* 10, 6116 (11 pages).
- Grasso, R., Ivanenko, Y.P., Zago, M., Molinari, M., Scivoletto, G., Castellano, V., Macellari, V., Lacquaniti, F., 2004. Distributed plasticity of locomotor pattern generators in spinal cord injured patients. *Brain* 127, 1019-1034.
- Grillner, S., 1981. Control of locomotion in bipeds, tetrapods, and fish. *Handbook of*

- Physiology II, 1179-1236.
- Harkema, S.J., Hurley, S.L., Patel, U.K., Requejo, P.S., Dobkin, B.H., Edgerton, V.R., 1997. Human lumbosacral spinal cord interprets loading during stepping. *Journal of Neurophysiology* 77, 797-811.
- Holstege, J.C., Kuypers, H.G., 1987. Brainstem projections to spinal motoneurons: An update. *Neuroscience* 23, 809-821.
- Ito, S., Nagoshi, N., Tsuji, O., Shibata, S., Shinozaki, M., Kawabata, S., Kojima, K., Yasutake, K., Hirokawa, T., Matsumoto, M., Takei, K., Nakamura, M., Okano, H., 2018. Lotus inhibits neuronal apoptosis and promotes tract regeneration in contusive spinal cord injury model mice. *eNeuro* 5 (16 pages).
- Ivanenko, Y.P., Cappellini, G., Dominici, N., Poppele, R.E., Lacquaniti, F., 2007. Modular control of limb movements during human locomotion. *Journal of Neuroscience* 27, 11149-11161.
- Ivanenko, Y.P., Cappellini, G., Solopova, I.A., Grishin, A.A., Maclellan, M.J., Poppele, R.E., Lacquaniti, F., 2013. Plasticity and modular control of locomotor patterns in neurological disorders with motor deficits. *Frontiers in Computational Neuroscience* 7, 123 (11 pages).
- Ivanenko, Y.P., d'Avella, A., Poppele, R.E., Lacquaniti, F., 2008. On the origin of planar covariation of elevation angles during human locomotion. *Journal of Neurophysiology* 99, 1890-1898.
- Ivanenko, Y.P., Grasso, R., Zago, M., Molinari, M., Scivoletto, G., Castellano, V., Macellari, V., Lacquaniti, F., 2003. Temporal components of the motor patterns expressed by the human spinal cord reflect foot kinematics. *Journal of Neurophysiology* 90, 3555-3565.
- Ivanenko, Y.P., Poppele, R.E., Lacquaniti, F., 2004. Five basic muscle activation patterns account for muscle activity during human locomotion. *Journal of Physiology* 556, 267-282.
- Ivanenko, Y.P., Poppele, R.E., Lacquaniti, F., 2006. Motor control programs and walking. *Neuroscientist* 12, 339-348.
- Ivanenko, Y.P., Poppele, R.E., Lacquaniti, F., 2009. Distributed neural networks for controlling human locomotion: Lessons from normal and sci subjects. *Brain Research Bulletin* 78, 13-21.
- Jordan, L., 1991. Brainstem and spinal cord mechanisms for the initiation of locomotion, In: Shimaura, M., Grillner, S., Edgerton, V.R. (Eds.), *Neurobiological basis of human locomotion*, Japan Scientific Societies Press, Tokyo, pp. 3-20.
- Kato, M., Murakami, S., Yasuda, K., Hirayama, H., 1984. Disruption of fore-and hindlimb

- coordination during overground locomotion in cats with bilateral serial hemisection of the spinal cord. *Neuroscience Research* 2, 27-47.
- Kawashima, N., Nozaki, D., Abe, M.O., Nakazawa, K., 2008. Shaping appropriate locomotive motor output through interlimb neural pathway within spinal cord in humans. *Journal of Neurophysiology* 99, 2946-2955.
- Kirshblum, S.C., Burns, S.P., Biering-Sorensen, F., Donovan, W., Graves, D.E., Jha, A., Johansen, M., Jones, L., Krassioukov, A., Mulcahey, M.J., Schmidt-Read, M., Waring, W., 2011. International standards for neurological classification of spinal cord injury (revised 2011). *The journal of spinal cord medicine* 34, 535-546.
- Kitamura, K., Fujiyoshi, K., Yamane, J., Toyota, F., Hikishima, K., Nomura, T., Funakoshi, H., Nakamura, T., Aoki, M., Toyama, Y., Okano, H., Nakamura, M., 2011. Human hepatocyte growth factor promotes functional recovery in primates after spinal cord injury. *PloS One* 6, e27706 (13 pages).
- Knutsson, E., Richards, C., 1979. Different types of disturbed motor control in gait of hemiparetic patients. *Brain* 102, 405-430.
- Lacquaniti, F., Grasso, R., Zago, M., 1999. Motor patterns in walking. *News in Physiological Sciences* 14, 168-174.
- Lamoth, C.J., Daffertshofer, A., Huys, R., Beek, P.J., 2009. Steady and transient coordination structures of walking and running. *Human Movement Science* 28, 371-386.
- Latash, M.L., 1999. On the evolution of the notion of synergy., In: Gantchev, G.N., Mori, S., Massion, J. (Eds.), *Motor control, today and tomorrow*, Academic Publishing House, Sofia, pp. 181-196.
- Leblond, H., L'Espérance, M., Orsal, D., Rossignol, S., 2003. Treadmill locomotion in the intact and spinal mouse. *The Journal of Neuroscience* 23, 11411-11419.
- Liddell, E., Phillips, C., 1944. Pyramidal section in the cat. *Brain* 67, 1-9.
- Loy, K., Bareyre, F.M., 2019. Rehabilitation following spinal cord injury: How animal models can help our understanding of exercise-induced neuroplasticity. *Neural Regeneration Research* 14, 405-412.
- Lunenburger, L., Bolliger, M., Czell, D., Muller, R., Dietz, V., 2006. Modulation of locomotor activity in complete spinal cord injury. *Experimental Brain Research* 174, 638-646.
- Luo, L., Callaway, E.M., Svoboda, K., 2018. Genetic dissection of neural circuits: A decade of progress. *Neuron* 98, 256-281.
- MacLellan, M.J., McFadyen, B.J., 2010. Segmental control for adaptive locomotor adjustments during obstacle clearance in healthy young adults. *Experimental Brain*

- Research 202, 307-318.
- Maier, I.C., Ichiyama, R.M., Courtine, G., Schnell, L., Lavrov, I., Edgerton, V.R., Schwab, M.E., 2009. Differential effects of anti-nogo-a antibody treatment and treadmill training in rats with incomplete spinal cord injury. *Brain* 132, 1426-1440.
- Martino, G., Ivanenko, Y., Serrao, M., Ranavolo, A., Draicchio, F., Casali, C., Lacquaniti, F., 2019. Locomotor coordination in patients with hereditary spastic paraplegia. *Journal of Electromyography and Kinesiology* 45, 61-69.
- Mathis, A., Mamidanna, P., Cury, K.M., Abe, T., Murthy, V.N., Mathis, M.W., Bethge, M., 2018. Deeplabcut: Markerless pose estimation of user-defined body parts with deep learning. *Nature Neuroscience* 21, 1281-1289.
- Matsuzaki, M., Ebina, T., 2020. Common marmoset as a model primate for study of the motor control system. *Current Opinion in Neurobiology* 64, 103-110.
- McKay, W.B., Ovechkin, A.V., Vitaz, T.W., Terson de Paleville, D.G., Harkema, S.J., 2011. Neurophysiological characterization of motor recovery in acute spinal cord injury. *Spinal Cord* 49, 421-429.
- Mulroy, S., Gronley, J., Weiss, W., Newsam, C., Perry, J., 2003. Use of cluster analysis for gait pattern classification of patients in the early and late recovery phases following stroke. *Gait and Posture* 18, 114-125.
- Nam, K.Y., Kim, H.J., Kwon, B.S., Park, J.W., Lee, H.J., Yoo, A., 2017. Robot-assisted gait training (lokomat) improves walking function and activity in people with spinal cord injury: A systematic review. *Journal of Neuroengineering and Rehabilitation* 14, 24 (13 pages).
- Okano, H., 2021. Current status of and perspectives on the application of marmosets in neurobiology. *Annual Review of Neuroscience* 44, 27-48.
- Orlovskii, G.N., Deliagina, T.G., Grillner, S., 1999. *Neuronal control of locomotion : From mollusc to man*. Oxford University Press, p. 322.
- Pepin, A., Ladouceur, M., Barbeau, H., 2003a. Treadmill walking in incomplete spinal-cord-injured subjects: 2. Factors limiting the maximal speed. *Spinal Cord* 41, 271-279.
- Pepin, A., Norman, K.E., Barbeau, H., 2003b. Treadmill walking in incomplete spinal-cord-injured subjects: 1. Adaptation to changes in speed. *Spinal Cord* 41, 257-270.
- Perez-Escudero, A., Vicente-Page, J., Hinz, R.C., Arganda, S., de Polavieja, G.G., 2014. Idtracker: Tracking individuals in a group by automatic identification of unmarked animals. *Nature Methods* 11, 743-748.
- Petras, J.M., 1967. Cortical, tectal and tegmental fiber connections in the spinal cord of the cat. *Brain Research* 6, 275-324.

- Poppele, R.E., Bosco, G., Rankin, A.M., 2002. Independent representations of limb axis length and orientation in spinocerebellar response components. *Journal of Neurophysiology* 87, 409-422.
- Prins, N.W., Pohlmeier, E.A., Debnath, S., Mylavarapu, R., Geng, S., Sanchez, J.C., Rothen, D., Prasad, A., 2017. Common marmoset (*Callithrix jacchus*) as a primate model for behavioral neuroscience studies. *Journal of Neuroscience Methods* 284, 35-46.
- Puentes, S., Kadone, H., Kubota, S., Abe, T., Shimizu, Y., Marushima, A., Sankai, Y., Yamazaki, M., Suzuki, K., 2018a. Reshaping of gait coordination by robotic intervention in myelopathy patients after surgery. *Frontiers in Neuroscience* 12, 99 (10 pages).
- Puentes, S., Kadone, H., Watanabe, H., Ueno, T., Yamazaki, M., Sankai, Y., Marushima, A., Suzuki, K., 2018b. Reshaping of bilateral gait coordination in hemiparetic stroke patients after early robotic intervention. *Frontiers in Neuroscience* 12, 719.
- Raineteau, O., Schwab, M.E., 2001. Plasticity of motor systems after incomplete spinal cord injury. *Nature Reviews: Neuroscience* 2, 263-273 (11 pages).
- Rossignol, S., Frigon, A., 2011. Recovery of locomotion after spinal cord injury: Some facts and mechanisms. *Annual Review of Neuroscience* 34, 413-440.
- Roussel, M., Lemieux, M., Bretzner, F., 2020. Using mouse genetics to investigate supraspinal pathways of the brain important to locomotion, In: Whelan, P.J., Sharples, S.A. (Eds.), *The neural control of movement model systems and tools to study locomotor function*, Elsevier, Amsterdam, pp. 269-313.
- Safavynia, S.A., Torres-Oviedo, G., Ting, L.H., 2011. Muscle synergies: Implications for clinical evaluation and rehabilitation of movement. *Topics in Spinal Cord Injury Rehabilitation* 17, 16-24.
- Sato, Y., Kondo, T., Shibata, R., Nakamura, M., Okano, H., Ushiba, J., in Press-a. Functional reorganization of locomotor kinematic synergies reflects the neuropathology in a mouse model of spinal cord injury. *Neuroscience Research*.
- Sato, Y., Kondo, T., Shinozaki, M., Shibata, R., Nagoshi, N., Ushiba, J., Nakamura, M., Okano, H., in Press-b. Markerless analysis of hindlimb kinematics in spinal cord-injured mice through deep learning. *Neuroscience Research*.
- Sato, Y., Kondo, T., Uchida, A., Sato, K., Yoshino-Saito, K., Nakamura, M., Okano, H., Ushiba, J., 2022. Preserved intersegmental coordination during locomotion after cervical spinal cord injury in common marmosets. *Behavioural Brain Research* 425, 113816 (9 pages).
- Schwab, M.E., Strittmatter, S.M., 2014. Nogo limits neural plasticity and recovery from

- injury. *Current Opinion in Neurobiology* 27, 53-60.
- Shah, P.K., Gerasimenko, Y., Shyu, A., Lavrov, I., Zhong, H., Roy, R.R., Edgerton, V.R., 2012. Variability in step training enhances locomotor recovery after a spinal cord injury. *European Journal of Neuroscience* 36, 2054-2062.
- Shimada, H., Kanai, R., Kondo, T., Yoshino-Saito, K., Uchida, A., Nakamura, M., Ushiba, J., Okano, H., Ogihara, N., 2017. Three-dimensional kinematic and kinetic analysis of quadrupedal walking in the common marmoset (*callithrix jacchus*). *Neuroscience Research* 125, 11-20.
- Squair, J.W., Gautier, M., Sofroniew, M.V., Courtine, G., Anderson, M.A., 2021. Engineering spinal cord repair. *Current Opinion in Biotechnology* 72, 48-53.
- Stetter, B.J., Herzog, M., Mohler, F., Sell, S., Stein, T., 2020. Modularity in motor control: Similarities in kinematic synergies across varying locomotion tasks. *Frontiers in Sports and Active Living* 2, 596063 (9 pages).
- Swanson, L.W., 1995. Mapping the human brain: Past, present, and future. *Trends in Neurosciences* 18, 471-474.
- Takeoka, A., Vollenweider, I., Courtine, G., Arber, S., 2014. Muscle spindle feedback directs locomotor recovery and circuit reorganization after spinal cord injury. *Cell* 159, 1626-1639.
- Tashiro, S., Nishimura, S., Iwai, H., Sugai, K., Zhang, L., Shinozaki, M., Iwanami, A., Toyama, Y., Liu, M., Okano, H., Nakamura, M., 2016. Functional recovery from neural stem/progenitor cell transplantation combined with treadmill training in mice with chronic spinal cord injury. *Scientific Reports* 6, 30898 (14 pages).
- Timoszyk, W.K., Nessler, J.A., Acosta, C., Roy, R.R., Edgerton, V.R., Reinkensmeyer, D.J., de Leon, R., 2005. Hindlimb loading determines stepping quantity and quality following spinal cord transection. *Brain Research* 1050, 180-189.
- Visintin, M., Barbeau, H., 1994. The effects of parallel bars, body weight support and speed on the modulation of the locomotor pattern of spastic paretic gait. A preliminary communication. *Spinal Cord* 32, 540-553.
- Wahl, A.S., Omlor, W., Rubio, J.C., Chen, J.L., Zheng, H., Schroter, A., Gullo, M., Weinmann, O., Kobayashi, K., Helmchen, F., Ommer, B., Schwab, M.E., 2014. Neuronal repair. Asynchronous therapy restores motor control by rewiring of the rat corticospinal tract after stroke. *Science* 344, 1250-1255.
- Wang, X., O'Dwyer, N., Halaki, M., 2013. A review on the coordinative structure of human walking and the application of principal component analysis. *Neural Regeneration Research* 8, 662-670.
- Wei, R.-H., Zhao, C., Rao, J.-S., Zhao, W., Zhou, X., Tian, P.-Y., Song, W., Ji, R., Zhang,

- A.-F., Yang, Z.-Y., Li, X.-G., 2018. The kinematic recovery process of rhesus monkeys after spinal cord injury. *Experimental Animals* 67, 431-440.
- Wernig, A., Muller, S., Nanassy, A., Cagol, E., 1995. Laufband therapy based on 'rules of spinal locomotion' is effective in spinal cord injured persons. *European Journal of Neuroscience* 7, 823-829.
- Willenberg, R., Steward, O., 2015. Nonspecific labeling limits the utility of cre-lox bred cst-yfp mice for studies of corticospinal tract regeneration. *Journal of Comparative Neurology* 523, 2665-2682.